ZHUANG, Chaoqun; WANG, Shengwei. Risk-based online robust optimal control of air-conditioning systems for buildings requiring strict humidity control considering measurement uncertainties. Applied Energy, 2020, 261: 114451.

https://doi.org/10.1016/j.apenergy.2019.114451

Risk-based online robust optimal control of air-conditioning systems for buildings requiring strict humidity control considering measurement uncertainties

Chaoqun Zhuang and Shengwei Wang*

Department of Building Services Engineering, The Hong Kong Polytechnic University, Kowloon, Hong Kong

Abstract: The total floor area and energy consumption of buildings or spaces requiring strict temperature and humidity control have been growing very fast worldwide. A major challenge for achieving energy-efficient control of air-conditioning systems in such applications is the measurement uncertainties underlying the systems' online optimal control decisions under ever-changing working conditions. This paper proposes a risk-based online robust optimal control strategy for multi-zone air-conditioning systems considering component performance degradation and measurement uncertainties. A risk-based online control decision scheme, as the core of the strategy, is developed for decision-making by compromising the failure risks and energy benefits of different control modes considering uncertainties in the information used. The proposed strategy is tested and implemented in a simulation platform based on an existing pharmaceutical industrial building. The results show that the proposed strategy made the optimal online control decisions, allowing for the measurement uncertainties. Compared with a commonly used control strategy, the proposed strategy achieved approximately 20% overall energy saving in the test period.

Keywords: risk-based control; online optimal control; cleanroom; air-conditioning; measurement uncertainty.

---

* Corresponding author: Shengwei Wang, email: beswwang@polyu.edu.hk

Nomenclature

a_1-a_2, b_1-b_2, c_1-c_4	coefficients
ACH	air change rates per hour
ADV	adaptive full-range decoupled ventilation
AHU	air-handling unit
COP_c	overall coefficient of performance of cooling system
COP_{he}	overall coefficient of performance of heating system
DV	dedicated outdoor air ventilation
e	white noise
E	electrical load (kW)
ΔE	dead band
h	enthalpy of air (kJ/kg)
IC	interactive control
L_w	length of the moving window
$\hat{m}$	measured value
m^r	true value
$\bar{m}$	moving averaged data
MAU	make-up air-handling unit
n_p	number of variables
PD	partially decoupled control
PDF	probability density function
P_f	failure risk
Q_{lat}	space latent cooling load (kW)
RH	relative humidity (%)
T	temperature (°C)
V	air volumetric flow rate (L/s)
w	humidity ratio (kg/kg)

Greek letters

β	sensor biases
Δ	standard deviation
α_t, γ_t	threshold value
λ	filtering weight factor
ρ	air density (kg/m^3)

Subscripts

cc	cooling coil
fh	outdoor air
fic	fictitious
he	heating system
inp	input
k,j	time instant
nb	net benefit
r	room
s	supply air
thr	threshold
out	outlet
otp	output

1 Introduction

Buildings or spaces requiring strict temperature and humidity controls, such as pharmaceutical cleanrooms, hospitals, semiconductor/microchip factories and museums (hereafter denoted as “cleanrooms” for brevity), are usually energy-intensive, having an average energy intensity 30-50 times greater than that of commercial buildings [1]. The annual energy intensity in cleanrooms has not seen a significant reduction over the last two decades [2]. The increased total floor area, high energy intensity and the complex system design and control of cleanrooms have raised widespread concerns over their rapidly growing energy consumption, leading to considerable interest in the potential for energy savings [3].

A good match between the sensible heat ratios (SHRs) of a space and the chosen air-conditioning system is vital for energy-efficient operation in cleanrooms, and closely depends on the ventilation strategy adopted. Existing ventilation strategies suitable for cleanrooms can be categorized as interactive control (IC) [4], dedicated outdoor air ventilation (DV) [5] and partially decoupled control (PD) strategies [6], according to the dehumidification demands of the make-up air-handling units (MAUs). However, these three existing ventilation strategies have their own limitations in cleanroom applications. IC and PD strategies involve sub-cooling and reheating processes to eliminate the coupling between temperature and humidity control loops, and these counteraction processes cause a considerable amount of energy waste [7]. The DV strategy can lead to high outdoor air cooling demands due to the introduction of intensive outdoor airflow [8]. To solve the above problems, the authors of this paper previously proposed a new “adaptive full-range decoupled ventilation” (ADV) strategy [9], which incorporates the advantages of various existing ventilation strategies. By avoiding sub-cooling and reheating as far as beneficial via the best use of the MAU for dehumidification, this strategy enables systems to operate at high energy efficiency across the full range of ambient and indoor load conditions.

The practical implementation of a ventilation strategy requires the proper design and selection of air-conditioning components. An appropriate system should meet both the sensible and latent loads not only under the design conditions but also a wide range of possible working conditions. The optimal design of air-conditioning components, such as fans, cooling coils and heaters, has been well addressed by ASHRAE [10]. In addition, considering the coordination among different components,

a probabilistic optimal design method facilitating the ADV strategy was also proposed [11], aiming to fulfill the requirements for optimal ventilation. The method proved able to provide the system with minimum life-cycle cost and excellent quality of service under various sources of uncertainties.

Besides appropriate design, a supervisory control strategy is also essential for implementing the ventilation strategy and achieving energy-efficient operation of cleanroom air-conditioning systems. For practical applications, the most appropriate operation/control mode should be carefully selected among several alternatives by means of online control, taking into account the ever-changing working conditions in practical situations reflected by real-time measurements. Many studies have shown that supervisory control strategies greatly improve the indoor comfort and thermal environment while minimizing the energy input under dynamic working conditions [12]. Nassif et al. [13] used a two-objective genetic algorithm to formulate a model-based supervisory control strategy for heating, ventilating, and air-conditioning (HVAC) systems, achieving an energy saving of 16% over an existing conventional air-conditioning system. West et al. [14] adopted an optimized supervisory model predictive control (MPC) for HVAC systems in commercial buildings. Average energy reductions of 19% and 32% were achieved in the two buildings, respectively. Ferreira et al. [15] applied a neural-network-based predictive control strategy for HVAC real-time control in an educational building, achieving a satisfactory thermal comfort level and 50% energy savings. However, the existing supervisory control strategies are generally developed for buildings requiring thermal comfort control, implying that the system relies on temperature-based control to remove indoor moisture. Adding humidity as an objective complicates the task of control [16], necessitating a supervisory control strategy for optimizing the simultaneous control of space temperature and humidity.

Due to the complexity of air-conditioning systems with counteractant processes and dynamic working conditions, errors and uncertainties in the measurements can lead to improper choices of system control modes, resulting in huge energy waste. For example, it has been reported that the measurement uncertainties of outdoor airflow can lead to 17% waste in cooling energy use and 43% waste in heating energy use [17]. The uncertainty in the occupancy measurements, meanwhile, can cause an increase of 18% in the total energy consumption [18]. Several online fault-tolerant control strategies have been developed and applied in air conditioning systems [19] to enable the systems to

operate at high efficiency and reliability in the presence of sensor faults/errors. Yang et al. [20] developed a fault-tolerant supervisory control scheme by correcting the faulty measurements and reconstructing the controller inputs. Wang and Chen [21] used neural network models to diagnose the measurement faults of airflow sensors, and realized the fault-tolerant control of outdoor airflow in the presence of sensor faults. Jin and Du [22] proposed a fault-tolerant control method to regulate the outdoor airflow and adjust the air-handling unit (AHU) supply air temperature, based on principal component analysis, the joint angle method and compensatory reconstruction. The basic idea of these online fault-tolerant control strategies is to detect and identify the faults of the control systems, and then recover or correct the sensor measurements. However, due to the propagation and interaction of different measurement uncertainties in the control process, it is difficult to fix or remove the bias faults in cases with simultaneous multiple sensor biases. Simultaneous multiple sensor biases are a common issue in practical operation as the physical properties of sensors change over time. As a result, the measurement uncertainties significantly influence the proper selection of control modes. One possible solution is to adopt a risk-based approach to support robust decision-making, “aiming for an optimal balance between acceptable levels of risk and the costs of further risk reduction” in the face of uncertain information [23]. This method provides flexibility for decision-makers in responding to possible changes that are uncertain or as yet unknown. The main advantage of this approach is that the risks and benefits of decisions are evaluated by quantifying the propagation of “aggregated uncertainties” instead of considering the uncertainty of each source. The risk-based approach for decision-making can be found in marketing [24], financial [23], ecological [25] and civil infrastructure [26] fields. For the energy-efficient operation of HVAC systems, a suitable decision should be made promptly based on the online measurements to avoid control failure and energy waste. However, currently, there is no quantification method of risks and benefits accounting for measurement uncertainties to ensure robust online decision-making and control for cleanroom air-conditioning systems.

This paper, therefore, proposes a risk-based online robust optimal control strategy for multi-zone cleanroom air-conditioning systems, which minimizes energy consumption in the face of measurement uncertainties and component degradation. The measurement uncertainties are considered indirectly by evaluating the risks and benefits of different control modes. The proposed

control strategy is developed by addressing the following two tasks: 1) identification of the correlations between different control modes for selecting the optimal control mode; 2) development of an online optimal decision-making scheme to evaluate the risks and benefits of different control modes, and selection of optimal modes for individual supply air-handing units (AHUs) allowing for measurement uncertainties. The correlations between different control modes are identified by comparing the air states of two modes under the given indoor load conditions, and are used to develop the risk evaluation models of the strategy prior to its actual operation. The failure risk of a control mode is evaluated online by analyzing the probabilities of both demanded and maximum outdoor air flowrates. The main innovation of this study is to develop a robust decision-making scheme for the proper selection of the control modes of air-conditioning systems. The potential risks/benefits resulting from the measurement uncertainties and component performance degradation are considered in the decision-making scheme, to ensure energy-efficient and reliable temperature and humidity controls. The proposed risk-based online robust optimal control strategy is tested and implemented in a dynamic simulation platform based on an existing pharmaceutical industrial building in a subtropical region.

2 Risk-based online robust optimal control of cleanroom air-conditioning systems

2.1 Typical air-conditioning system configuration and ventilation modes

To describe the basic principle of the proposed risk-based online robust optimal control strategy, a typical cleanroom air-conditioning system configuration (ISO class 8 [27]), i.e. an MAU and multiple AHUs serve for multiple zones, is selected as shown in Fig. 1. The MAU consists of a fan, a cooling coil and filters for handling the outdoor air. The AHU consists of a fan, a cooling coil, an electric heater and filters for handling the supply air. The outside and recirculated air are filtered across high-efficiency particulate air (HEPA) filters to remove airborne particles. Different types of sensors are installed in the duct or components to record the air states. In this study, the cleanliness of cleanrooms is ensured by assigning the system with high supply air flowrates and duct pressure drops. The supply air flowrate of cleanrooms is designed as 20 air change rates per hour (ACH) [28] to ensure indoor contamination levels of ISO class 8 [27], which is significantly higher than that for typical commercial buildings [29] or office buildings [30] where the emphasis is on thermal comfort control (i.e. the supply air flowrate is typically less than 5 ACH). The settings for the pressure drop in the

ducts are high with consideration of the installation of HEPA filters. Note that the control strategy for cleanrooms with higher cleanliness requirements (i.e. ISO class 3-7) is not in the scope of this study, as the system configuration and airflow pattern are different in such cases (i.e. utilizing fan filter units (FFUs) for unidirectional airflow).

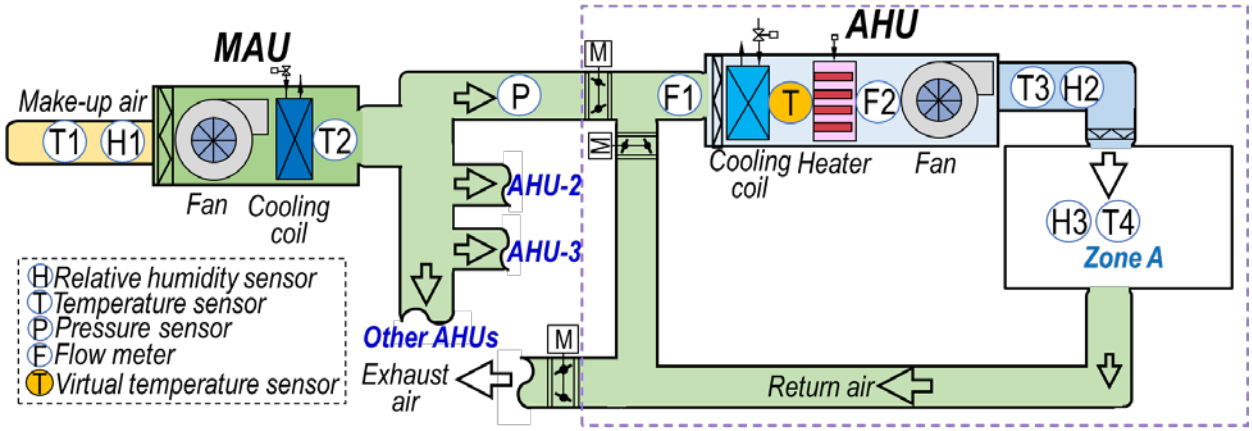

Fig. 1 System configuration of a typical cleanroom air-conditioning system.

Three ventilation modes, namely IC, DV and PD can be used for cleanroom ventilation control. These modes all adopt the feedback closed-loop control. The description and limitations of the three ventilation modes are summarized in Table 1. The PD mode is regarded as a suitable substitute for the IC mode because it is energy-efficient under part-load conditions due to its decoupled temperature and humidity control loops. The PD and DV modes have their own limitations and advantages under different working conditions and the online selection of the choice between them is still an unmet challenge.

Table 1 Comparision of three ventilation modes [9]

Mode	Description	Limitations
Interactive control (IC)	o Outdoor air is treated near the indoor air enthalpy with the minimum required outdoor airflow. o The AHU handles all indoor latent and sensible load.	The counteraction between cooling and reheating for humidity and temperature controls
Partially decoupled control (PD)	o Outdoor air is treated below the indoor air dewpoint with the minimum required outdoor airflow.	The counteraction between cooling and reheating for humidity and temperature controls

	o Under high indoor latent load conditions, the MAU handles part of the indoor sensible and latent load while the AHU handles the rest. o Under low indoor latent load conditions, the MAU handles all of the indoor latent load and part of the sensible load and while the AHU handles the rest of the indoor sensible load.	under high indoor latent load conditions
Dedicated outdoor air ventilation (DV)	o Outdoor air is treated below the indoor air dewpoint with adjustable outdoor airflow. o The outdoor airflow is adjusted according to the indoor latent load. o The MAU handles all of the indoor latent load and part of the sensible load and while the AHU handles the rest of the indoor sensible load.	High ventilation energy demand under hot-humid outdoor air conditions

2.2 Overall structure of risk-based online robust optimal control strategy

Fig. 2 shows the overall structure of the risk-based online robust optimal control strategy, which involves decision-making approaches and adaptive control at two levels. At the local level, local feedback process controllers control the process outputs at their optimum or predetermined set-points according to the control mode determined at the upper level. At the upper level, the optimal control modes for individual AHUs are determined by the "online optimal decision-making scheme". The scheme compares the risks/benefits of different control modes and selects the optimal mode for each AHU, to achieve energy-efficient and reliable temperature and humidity controls. The control modes available to the system are PD and DV. The differences of control logics between the two modes are highlighted by the different line styles in Fig. 2.

Control mechanism of PD mode: The fan speed and cooling coil valve opening of the MAU are modulated by pressure and temperature controllers respectively to maintain the air static pressure (i.e. at the sensor location) and outlet temperature at a lower limit (i.e. much lower than indoor air dew-point temperature). The heater output of each AHU is modulated (by a humidity controller) to control the space relative humidity within its allowable range. The cooling of each AHU is modulated (by a temperature controller) to control the supply air temperature at its set-point ($T_{AHU,sp}$). The supply air temperature set-point ($T_{AHU,sp}$) is adjusted (by a temperature reset controller) according to the indoor air temperature. The make-up air damper for each AHU is modulated (by an airflow controller) to control the outdoor airflow at its lower limit ($V_{fh,PD}$), which is the minimum outdoor airflow rate

required for maintaining the acceptable indoor air quality or space positive pressure.

Control mechanism of DV mode: The DV mode differs from the PD mode in two ways. First, the setpoint of outdoor airflow ($V_{fh,DV}$) is adjusted (by a humidity controller) according to the indoor air relative humidity (i.e. indoor latent load). Second, the heating of each AHU is seldom used due to the fully decoupled temperature and humidity control loops.

To select the optimal control mode online, two objectives of the online optimal decision-making scheme need to be addressed, including 1) risk and benefit evaluation of different control modes, and 2) selection of optimal control mode. The need and benefits of developing the decision-making scheme are outlined in Section 2.2. The mechanism of optimal control mode selection is illustrated in Section 2.3. The development of adaptive models to identify the correlations between different modes considering uncertainties for risk and benefit evaluation is presented in Section 2.4.

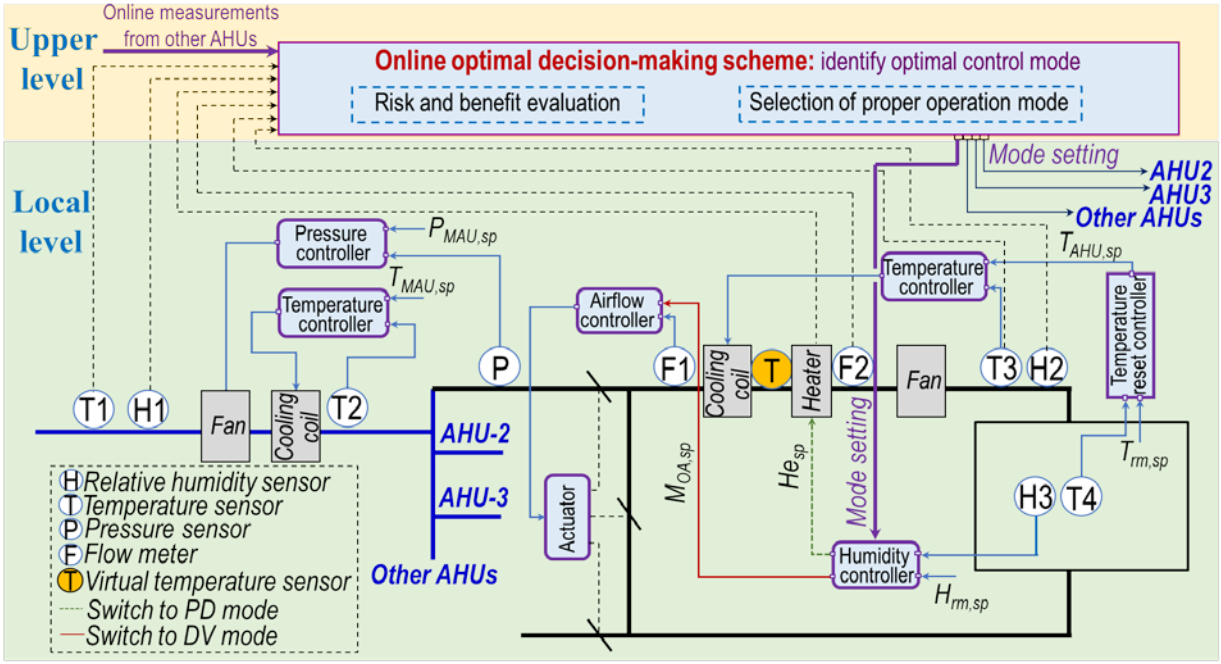

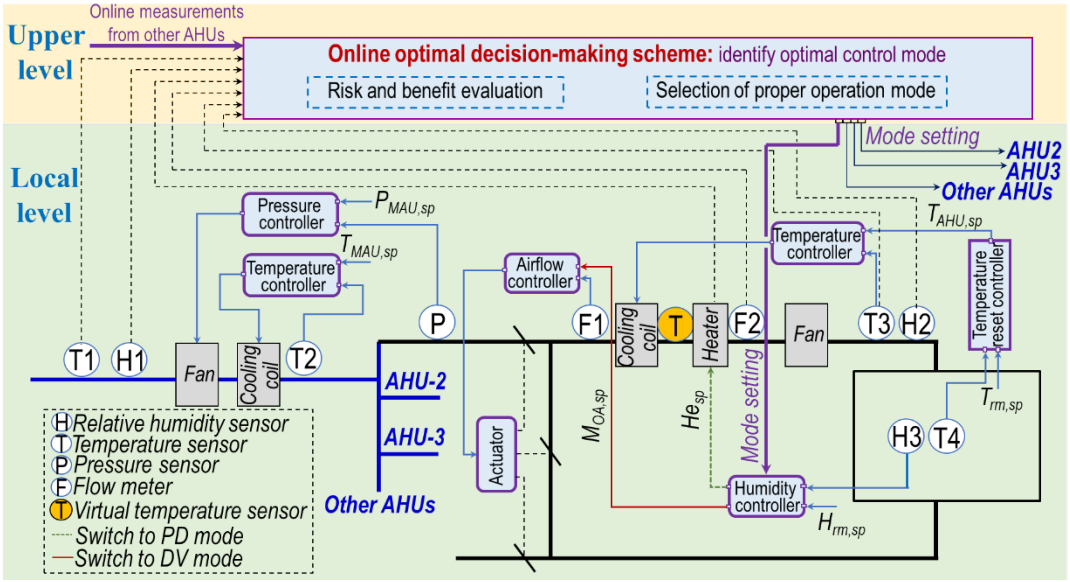

Fig. 2 Overall structure of the risk-based online robust optimal control strategy

2.3 The need and benefits of risk-based decision-making

Multiple control modes are available in many control systems. However, because the optimal control mode varies according to the working conditions, its identification is an important challenge, especially when the systems suffer from component performance degradation and measurement uncertainties. Fig. 3 presents a typical case for cleanroom air-conditioning control systems [9], which shows the optimal control modes under different indoor load regions. The figure was plotted under a given outdoor air condition, assuming that the component capacities can satisfy the cooling demands. Where, the SHR is defined as the sensible heat or cooling load divided by the total heat or cooling load. Under the same total cooling load, a lower SHR indicates that a higher moisture load needs to be handled. The SHR is used to represent the load characteristics in cleanrooms. When a space has a comparatively high SHR (Region 1), both the PD and DV modes have the same energy performance, because all of the indoor latent load can be removed by the MAU to avoid the need for overcooling and reheating counteraction processes. When a space has a medium SHR (Region 2), the DV mode has outperforms the PD mode, because the energy saving (i.e. by avoiding counteraction processes) exceeds the energy waste (i.e. by introducing intensively high-enthalpy outdoor air). When a space has low SHR (Region 3), PD outperforms DV, because the energy saving of the latter is less than the energy waste. With the decrease of outdoor air enthalpy, the boundary line between Region 2 and 3 moves down and the area of Region 2 increases, eventually subsuming Region 3.

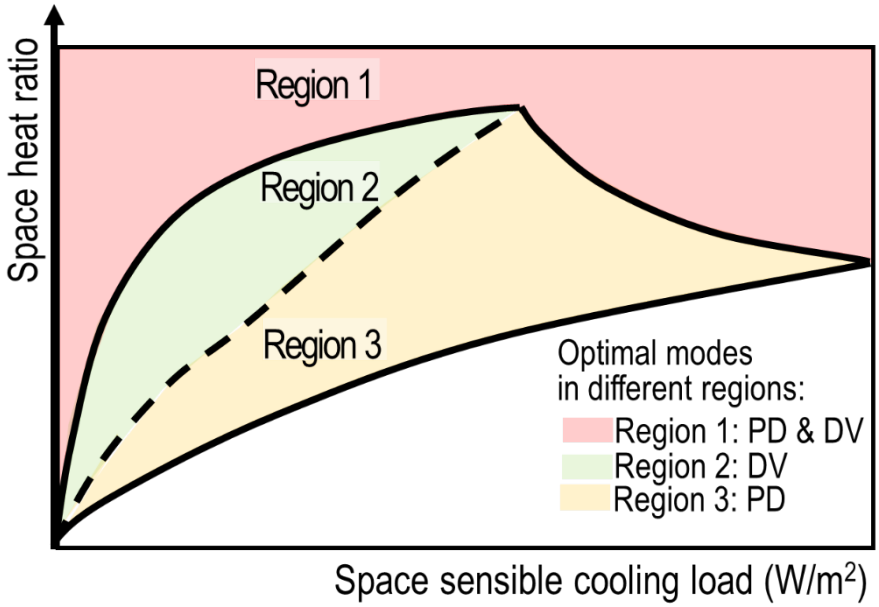

Fig. 3 Optimal modes under different indoor load regions and a given outdoor air condition [9]

The major task of the proposed online control strategy is to identify the optimal control mode (i.e. DV or PD), which is defined as the mode that enables the system to operate at the highest energy efficiency and reliability. However, the actual performance of a system is significantly influenced by the actual MAU cooling capacity and load. Fig. 4A shows the required MAU cooling demand under different latent cooling load (Q_{lat}) conditions for multiple zones (using three zones as an example). The conservative mode is a safe mode that can always maintain acceptable control and moderate energy consumption because the MAU cooling demand is kept at a low level (lower than the MAU cooling capacity) in all three regions. The aggressive mode is a highly economical but risky mode, which offers satisfactory energy performance over all three regions but carries a high failure risk due to high ventilation cooling demands. The MAU cooling demand is maintained at a low level in Regions 1 and 3 while the cooling demand increases with the increase of space latent load in Region 2. In real applications, an MAU usually treats and supplies the outdoor air to multiple AHUs. Therefore, the control mode should be properly set to avoid control failure (i.e. MAU demand exceeding its capacity), especially when the latent loads of all zones are in Region 2. The optimal mode is determined based on the online decision-making scheme by selecting between conservative and aggressive control modes, to avoid control failure while minimizing energy consumption. For instance, if the component cooling capacity can meet the required cooling demand under the aggressive mode, this mode is optimal as its energy performance is better than that of the conservative

mode. In contrast, if the component cooling capacity cannot meet the required cooling demand under the aggressive mode, the conservative mode is optimal due to its high reliability (i.e. the aggressive mode will consume more energy when control failure occurs). Fig. 4B shows the four possible operation options when the latent loads of all zones are high (i.e. in Region 2). For Option 1, all zones adopt the aggressive mode (DV mode). Therefore, high MAU cooling demand is required for dehumidification purposes, which exceeds the MAU cooling capacity and results in control failure. For the other three options, one zone adopts the conservative mode and the other zones adopt the aggressive mode. Options 2-4 all ensure successful system operation, although the optimal option (endowing systems with the highest energy-efficiency and reliability) must be determined according to their actual energy performance, which is further elaborated in Section 3.3. In real applications, the actual cooling demand and capacity are difficult to accurately estimate due to component performance degradation and measurement uncertainties, which significantly influences the proper selection of control modes. To avoid the failure of the selected control modes, a decision-making scheme considering the possible uncertainties is needed.

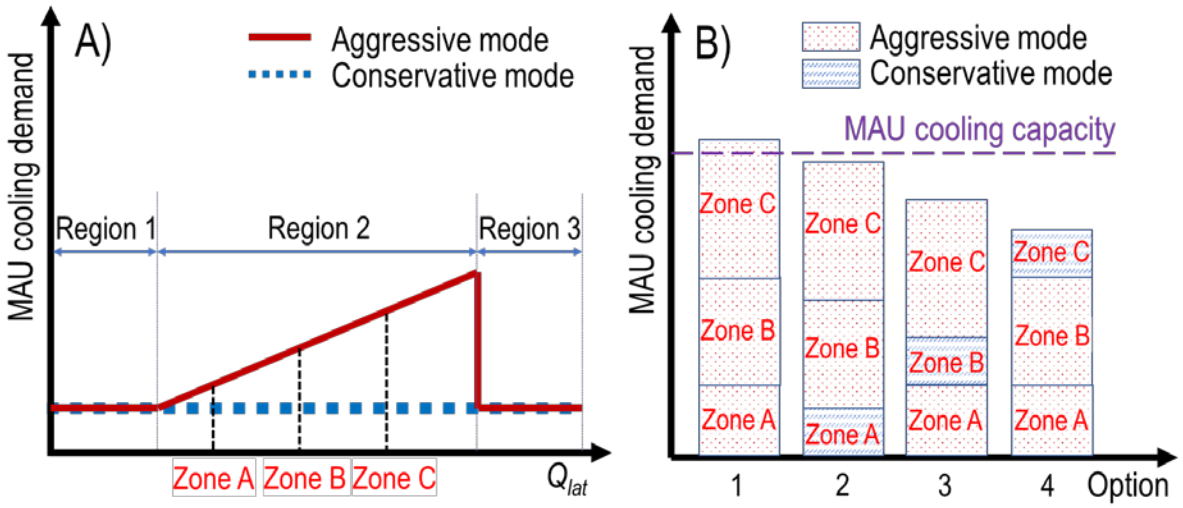

Fig. 4 Problems affecting the selection of control modes for multiple zones

(A. MAU cooling demand under different latent load conditions; B. MAU cooling demand versus MAU cooling capacity in different options)

2.4 Mechanism of risk-based control mode selection

A compromise between the failure risks and energy benefits is made using a probabilistic approach for selecting between the aggressive and the conservative control modes. Such a selection is

commonly faced in applications at medium/high indoor load conditions (e.g. pharmaceutical cleanrooms and labs), especially in humid climates. The mechanism of compromising in making a robust online decision in this situation is illustrated in Fig. 5. The optimal control mode of individual AHUs is determined as a compromise between the energy benefit in case of success and the energy waste in case of failure. When the cooling demand is low (i.e. lower than cooling capacity), adopting the aggressive mode (DV) offers a significant energy benefit (E_b) compared with the conservative mode (PD) if the decision is correct. However, when the cooling demand becomes higher (i.e. higher than cooling capacity), the failure risk (P_f) of adopting the aggressive mode increases. The aggressive mode becomes unachievable in practice when the component cooling capacity is lower than its cooling demand. There will be much energy waste (E_w) if the decision is wrong, resulting in control failure (denoted as "aggressive mode failure"). The optimal switching point for the control mode should be the point at which Q_D=Q_C in principle, but the actual estimation of this point is itself uncertain due to the uncertainties in estimating the cooling demand and cooling capacity. When the selected switching point moves to the right, the failure risk (P_f) increases, as shown in the figure.

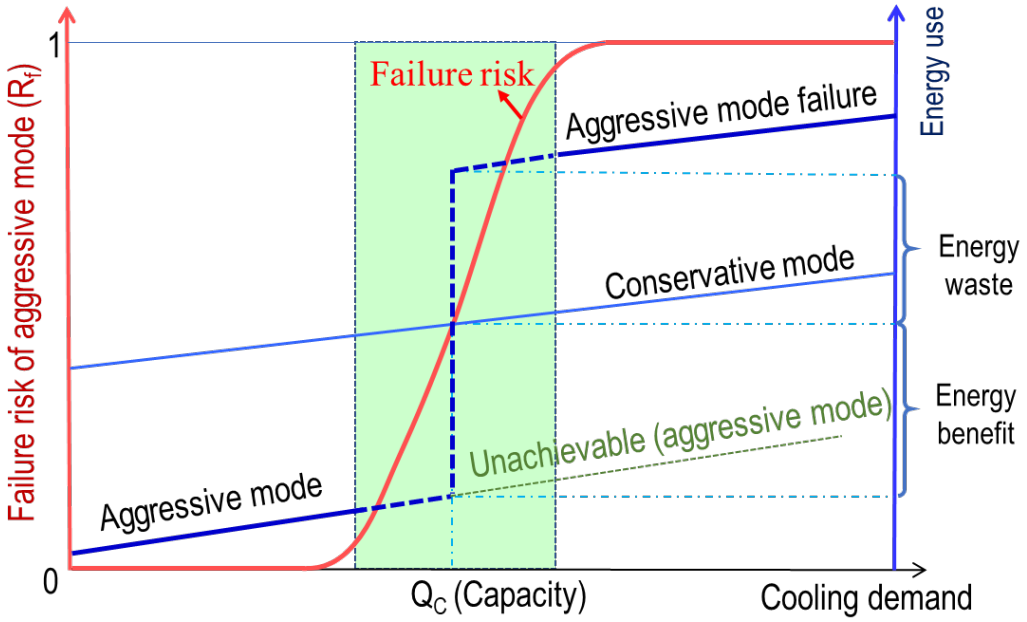

Fig. 5 Probabilistic optimal decisions for selecting the optimal control mode

The compromise-based decision will keep the system in the aggressive control mode until the expected net energy benefit (E_{nb}) is less than a predetermined threshold (E_{thr}) as shown by Eq. 1. Here, E_{nb} is a weighted value considering the energy benefit (E_b)/waste (E_w) and the corresponding

modes' probabilities of success (R_s)/failure (R_f). A dead band (ΔE) is introduced to avoid situations where switching between the two modes is too frequent. The evaluation of energy benefit/waste and their probabilities is further elaborated in Section 3.3.

$$\begin{cases} E_{nb} = \int E_b R_s - E_w R_f \geq E_{thr} + \frac{\Delta E}{2} & \rightarrow aggressive\ mode \\ E_{nb} = \int E_b R_s - E_w R_f \leq E_{thr} - \frac{\Delta E}{2} & \rightarrow conservative\ mode \end{cases} \quad (1)$$

2.5 Adaptive models for risk evaluation considering component performance degradation and measurement uncertainties

Due to the component performance degradation and measurement uncertainties, the actual cooling capacity (Q_c) and cooling demand (Q_d) are challenging to accurately estimate through direct measurements. In this study, the maximum ($V_{fh,max}$) and the demanded outdoor air flowrate (V_{fh}), which represent the correlations between Q_c and Q_d as described by Eq. 2, are used to evaluate the failure risks of a prospective decision. Here, $V_{fh,max}$ is the maximum outdoor airflow rate that the MAU can handle under constant outlet temperature (i.e. at dew-point). V_{fh} is the outdoor airflow that the system currently requires. For the conservative mode, there is no risk that the demanded outdoor airflow will be higher than $V_{fh,max}$ because the demanded outdoor airflow ($V_{fh,PD}$) is always maintained at its lower limit. For the aggressive mode, $V_{fh,DV}$ is adjusted according to the indoor latent load, and can exceed its lower limit. Hence there is a risk that the demanded outdoor airflow will be higher than $V_{fh,max}$ especially when the indoor latent load and outdoor air enthalpy are high. When the system operates in the aggressive mode, the demanded outdoor air flowrate ($V_{fh,DV}$) can be directly measured. The critical issue is to evaluate the value of $V_{fh,DV}$ at which the system decides to shift from the conservative mode to the aggressive mode. The correlations between different control modes can be identified by comparing the air states of two modes under the same or similar indoor load conditions (i.e. similar supply air and indoor air states) as elaborated in Section 3.2.

$$\frac{V_{fh,max}}{V_{fh}} = \frac{Q_c}{Q_d} \quad (2)$$

Adaptive models (Eqs. 3 and 4) are developed to predict the $V_{fh,max}$ and the $V_{fh,DV}$ using measured data. The outdoor air enthalpy, h_{fh}, which is a function of the measured outdoor air temperature and relative humidity, is used to predict the $V_{fh,max}$. The adaptive models are built by assuming the component capacities are unchanged in a short period. A "fictitious" AHU cooling coil outlet

temperature ($T_{fic,PD}$, in the conservative mode) is introduced to predict the $V_{fh,DV}$ in the aggressive mode. $T_{fic,PD}$ is estimated by assuming a virtual temperature sensor located on the AHU cooling coil outlet, as marked in Fig. 1 and Fig. 2. $V_{fh,DV}$ and $T_{fic,PD}$ have a negative linear correlation as described in Appendix A. $T_{fic,PD}$ is a function of the measured AHU supply air temperature (T_s) and heating load of heaters (Q_{he}) as shown in Eq. 5, where, a_1, a_2, b_1 and b_2 are correlation coefficients with certain distributions needed to be quantified, aggregating the component performance degradation, measurement biases and noises. $T_{rise,fan}$ and m_s are the air temperature rise (K) due to the fan motor and supply mass airflow (kg/s), respectively, which are constant for a constant air volume (CAV) system. Q_{he} is evaluated using the heater output and rated power (kW).

$$V_{fh,max} = \frac{a_1}{h_{fh}} + a_2 \tag{3}$$

$$V_{fh,DV} = b_1 T_{fic,PD} + b_2 \tag{4}$$

$$T_{fic,PD} = T_s - T_{rise,fan} - \frac{Q_{he}}{m_s} = f(T_s, Q_{he}) \tag{5}$$

The coefficients of the adaptive models are fitted offline using measured data. Fig. 6 (A) shows the correlation between h_{fh} and $V_{fh,max}$, which is affected by the performance degradation of the MAU. The solid curve represents the performance of a new MAU and the dashed curve represents the degraded MAU affected by the aging/fouling. The correlations are obtained by assuming that the outlet temperature (i.e. at the dew-point) of the MAU cooling coil is constant (i.e. 13 °C). Fig. 6 (B) shows the correlations between $T_{fic,PD}$ and $V_{fh,DV}$ of different zones. For zones with the same volume, the trends of $T_{fic,PD}$ and $V_{fh,DV}$ should be the same, as shown by the solid red line if no uncertainties are involved. The correlations are obtained by assuming that the temperature rise due to heat generation from the AHU fan motor is constant and identical under the same supply air flowrate. However, due to measurement uncertainties in each zone, the slope and intercept of the lines differ between zones. The measurement uncertainties (noises and biases) are thus aggregated into the adaptive models by identifying the model coefficients. The coefficients of the adaptive models are updated regularly, considering the changes in the uncertainties and the component performance degradation.

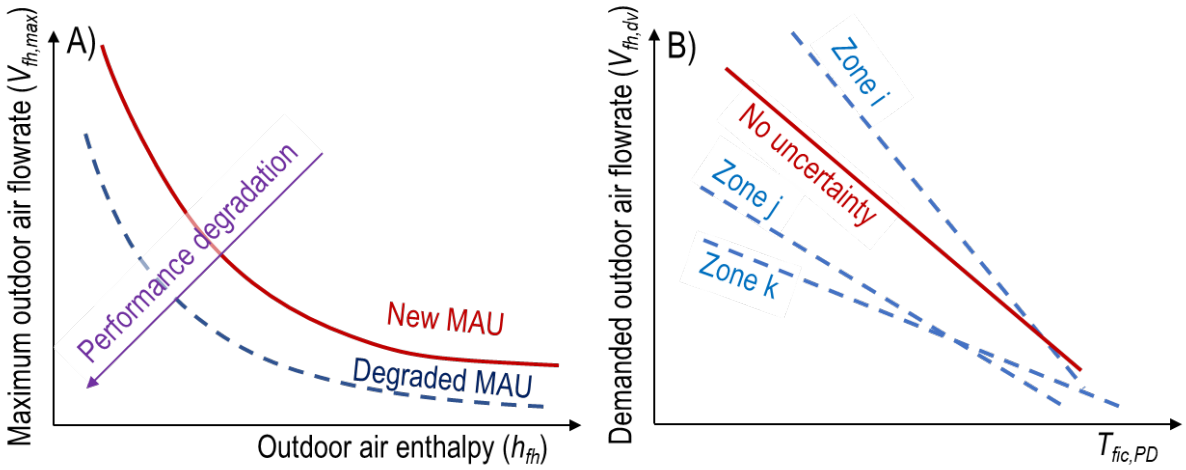

Fig. 6 Adaptive models considering component performance degradation and measurement uncertainties

(A. outdoor air enthalpy versus maximum outdoor air flowrate; B. fictitious AHU cooling coil outlet temperature of conservative mode versus demanded outdoor air flowrate of aggressive mode)

3 Detailed steps of the risk-based online robust optimal control strategy

The detailed steps of the proposed risk-based online robust optimal control strategy considering the measurement uncertainties are shown in Fig. 7. The first of the three main steps is to remove the outliers and identify the steady-state measurements. The second step is to identify the coefficients of the adaptive models. Both the maximum and demanded outdoor air flowrate models are fitted in advance using the measured data. The MAU fan energy model can be fitted using measurements or manufacturers' performance data. These models are updated regularly considering the measurement uncertainties and component performance degradation. The third step is to evaluate the risks and benefits of each control mode based on the possibilities of both the maximum and demanded air flowrate, as well as the predicted fan energy power, for online decision-making. These steps are elaborated in detail in the subsections below.

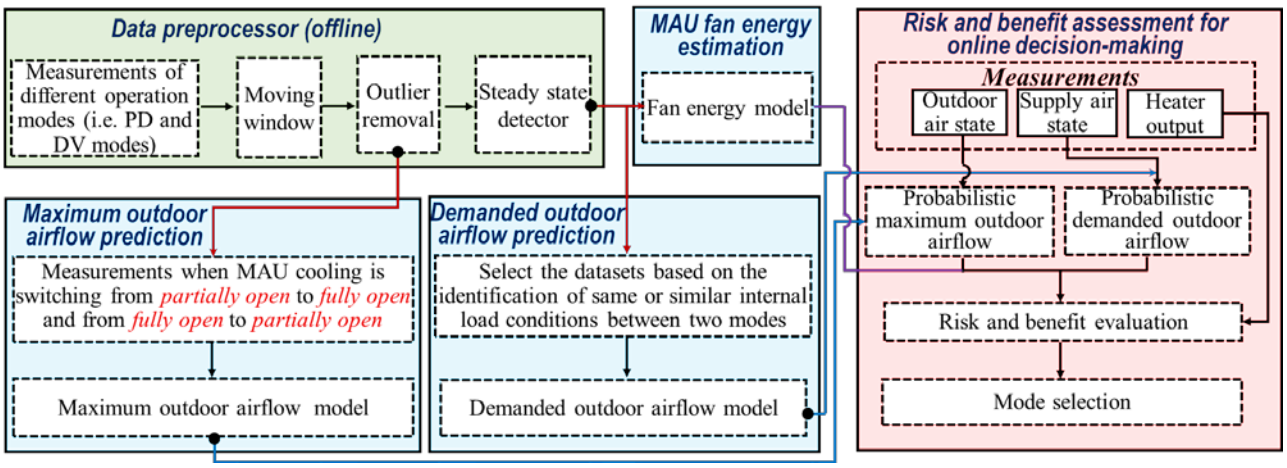

Fig. 7 Detailed steps of risk-based online robust optimal control under measurement uncertainties

3.1 Outlier removal and steady-state identification

The measurements of temperature, humidity and air flowrate are highly susceptible to measurement noises, outliers, and biases [31]. Taking measurement noises and biases into account, the reading given by a sensor is described by

$$\hat{m} = m^r + e + \beta \tag{6}$$

where m^r is the true value of $\hat{m}$, e is white noise and β denotes the sensor biases. A moving window is used to reduce the effects of measurement noise and outliers, which is defined as a matrix with dimension $L_w \times n_p$ as shown in Eq. 7. L_w and n_p are the length of the moving window and the number of variables, respectively. k is the time instant. To simplify the data preprocessing, two conventional assumptions are made [23]: *i)*. Measurement noises are normally distributed. *ii)*. Measurement biases are unknown constants within the moving window.

$$\begin{bmatrix} m_{1,1} & m_{2,1} & \cdots & m_{n_p,1} \\ m_{1,2} & m_{2,2} & & m_{n_p,2} \\ \vdots & & \ddots & \vdots \\ m_{1,L_w} & m_{2,L_w} & \cdots & m_{n_p,L_w} \end{bmatrix}_k \tag{7}$$

Fig. 8 shows the flowchart of the outlier removal and steady-state identification. The three-sigma rule [32] is used to detect the outlier and steady-state within a moving window. If the measurements in the defined window are more than three scaled median absolute deviations (MAD) away from the median, the system may experience significant dynamics or the measurements are outliers. The dynamic measurements and outliers are then removed from the datasets. A further step of the dynamic filter is applied. If the standard deviation (δ) of a measurement from the mean value in the window

is larger than a threshold α_t, this measurement is regarded as dynamic and removed from the database. Because the measurement noise e has zero expectation, $\bar{m}$ will be close to ($m^r + \beta$) when L_w is large enough as shown in Eq. 8. Taking the mean value ($\bar{m}$) of the moving windows reduces the influence of sensor noises.

$$\bar{m}_k = m_k^r + \mathbb{E}(e) + \beta \approx m_k^r + \beta,\ e \sim N(0, \sigma^2) \tag{8}$$

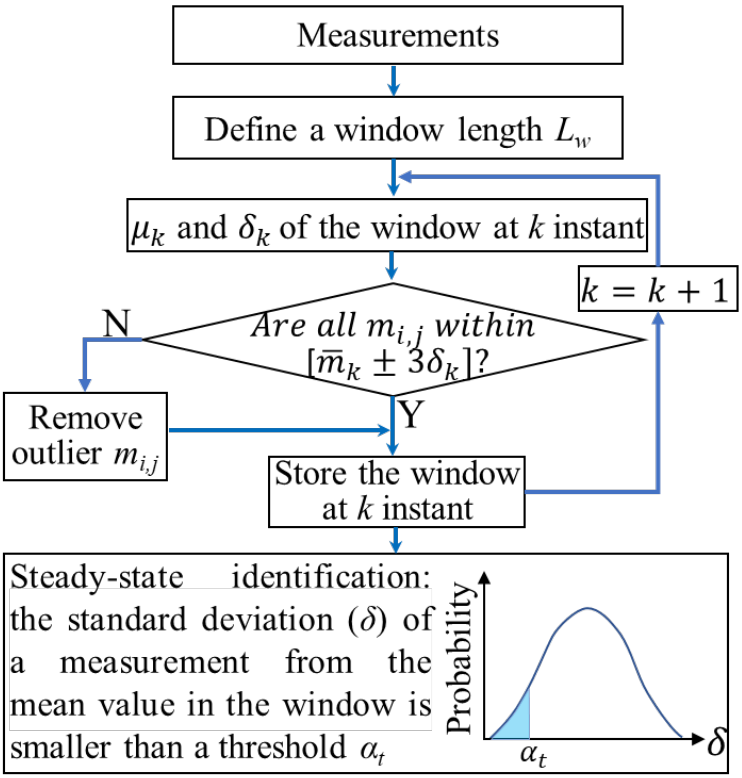

Fig. 8 Outlier removal and steady-state identification

3.2 Identification of model coefficients

In this study, both the maximum and demanded outdoor air flowrate models are modelled "probabilistically" and their coefficients are identified in specific ranges (confidence intervals) with proper distributions rather than deterministic values. The MAU fan model is a regular deterministic model and its coefficients are deterministic constants. A probabilistic model is necessary because both the maximum and demanded outdoor air flowrate have significant implications for the selection of the control mode, as shown in Section 2.5, and the risk of each prospective mode due to these erratic flowrate data needs to be carefully addressed.

Maximum outdoor airflow model: The data for fitting this model (i.e. Eq. 3) are selected based on the assumption that when the MAU cooling valve is switched from *partially open to fully open* and vice

versa, the MAU capacity is equal to its measured cooling load. Fig. 9 shows an actual profile of the cooling valve position of an MAU in a pharmaceutical cleanroom subsystem during a summer day. Due to the insufficient capacity of the MAU, its cooling valve was fully open between 12:20 and 13:40 and between 17:00 and 18:30. Vf_1, Vf_2, Vf_3 and Vf_4 are thus the switching points as mentioned above. The corresponding data of the outdoor airflow and outdoor air states are selected to form the model training database.

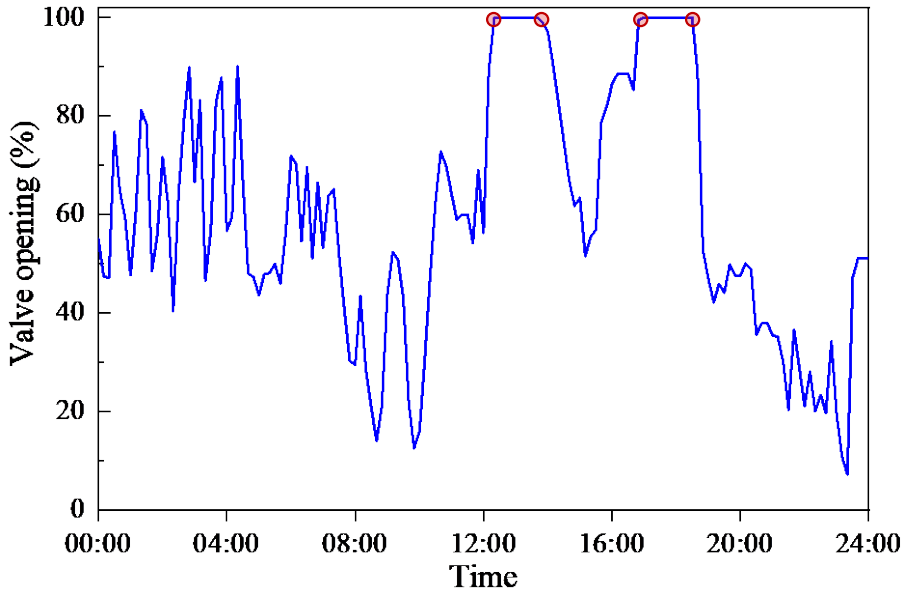

Fig. 9 Opening status of the MAU cooling valve on a summer working day

Demanded outdoor airflow model: The data for fitting this model (Eq. 4) are selected by identifying the similarity of the indoor load conditions between the two modes, which involves two steps. In the first step, the "distances" (Eq. 9) between two sets of measurements, taken under the aggressive mode and the conservative mode respectively, are calculated. The distances are used to quantify the similarities of the indoor load conditions under the two control modes. Here, T_r and T_s are room and supply air temperature (°C). RH_r and RH_s are the room and supply air relative humidity (%). In the second step, the sets of measurements with the distances lower than a threshold γ_t are selected and used as visible operational states in the two different control modes under the same indoor load conditions. The corresponding data of heater output, supply air temperature and outdoor air flowrate are selected to form the model training database.

$$d_k = \sqrt{\left(\hat{T}_{r,PD} - \hat{T}_{r,DV}\right)_k^2 + \left(\widehat{RH}_{r,PD} - \widehat{RH}_{r,DV}\right)_k^2 + \left(\hat{T}_{s,PD} - \hat{T}_{s,DV}\right)_k^2 + \left(\widehat{RH}_{s,PD} - \widehat{RH}_{s,DV}\right)_k^2} \quad (9)$$

MAU fan energy model: The MAU fan power is approximated as a three-order polynomial function of the volumetric flowrate as shown in Eq. 10, where c_1, c_2, c_3 and c_4 are deterministic constants fitted using the measured outdoor flowrate (V_{fh}) and fan power (P_{fan}). In real applications, if the fan power data are not available, the fan power can also be estimated using the manufacturer's performance data [33]. This will not seriously affect the decision-making process because the energy consumed by the fan motor is much smaller than cooling/heating energy. The accuracy of fan energy estimation thus has little impact on the final decision.

$$P_{fan} = c_1 V_{fh}^3 + c_2 V_{fh}^2 + c_3 V_{fh} + c_4 \quad (10)$$

3.3 Quantification of risks/benefits and selection of optimal control mode

As mentioned in Section 2.4, the critical issue when selecting the optimal operation/control mode is to evaluate the expected net energy benefit ($E_{nb,}$ Eq. 1). This is a weighted value considering the energy benefit (E_b)/waste (E_w) and the corresponding success (R_s)/failure probabilities (R_f) of the modes, elaborated as follows.

Energy benefit (E_b) and waste (E_w) evaluation: The energy benefit (E_b) of using the aggressive mode can be calculated using Eq. 11. The first two terms represent the additional energy uses (MAU cooling and fan energy) compared with the conservative mode, due to the introduction of excessive outdoor airflow. The third term represents the energy saving due to the prevention of overcooling and reheating. The energy waste (E_w) when using the aggressive mode can be calculated using Eq. 12. When failure occurs, a "penalty" is introduced by assuming that 100% outdoor airflow would be induced (i.e. the outdoor air damper is fully open). In addition, the AHUs resort to overcooling and reheating processes to ensure the indoor environment can be controlled within the allowable range. Here, h_r (*kJ/kg*) is the room air enthalpy under the design conditions (i.e. 23 °C, 63%). ρ_{fh} and ρ_s are the air density (kg/m^3) of the outdoor air and supply air, respectively. COP_c and COP_{he} are the overall coefficient of performance of the cooling system and heating system, assumed to be constant as 2.5 and 1.0, respectively. $V_{fh,full}$ is the 100% outdoor air flowrate (*L/s*), which is equal to the supply air flowrate (V_s). P_{fan} is a function of the volumetric flowrate, as shown in Eq. 10.

$$E_b = \frac{\rho_{fh}(V_{fh,DV} - V_{fh,PD})(h_{fh} - h_r)}{COP_C} + [P_{fan}(V_{fh,DV}) - P_{fan}(V_{fh,PD})] + \rho_s V_s Q_{he}\left(\frac{1}{COP_C} + \frac{1}{COP_{he}}\right) \quad (11)$$

$$E_w = \frac{\rho_{fh}(V_{fh,full}-V_{fh,PD})(h_{fh}-h_r)}{COP_C} + [P_{fan}(V_{fh,full}) - P_{fan}(V_{fh,PD})] \quad (12)$$

Evaluation of success and failure probabilities: The failure probability (R_f) and success probability (R_s) of the different control modes are estimated using Eqs. 13-14. The failure probability refers to the probability that the maximum outdoor air flowrate ($V_{fh,max}$) will be less than the demanded outdoor air flowrate ($V_{fh,DV}$), while the success probability is the probability that $V_{fh,max}$ will be higher than the $V_{fh,DV}$. Here, f_1 and f_2 are probability density functions (PDFs) of $V_{fh,max}$ and $V_{fh,DV}$ respectively under a certain working condition, obtained from the adaptive models (Eqs. 3-4). When the system adopts the aggressive mode (Fig. 10A), R_f is the integral of f_1 over the range between -∞ and the measured outdoor airflow ($\hat{V}_{fh}$). R_s is the integral of f_1 over the range between $\hat{V}_{fh}$ and +∞. When the system operates in the conservative mode (Fig. 10B), R_f is the overlap area of f_1 and f_2. R_s is the integral of $[f_2\text{-}min\ (f_1, f_2)]$.

$$R_s = \begin{cases} \int f_1(V_{fh,DV})\, dV_{fh,DV} \quad |V_{fh,DV} < \hat{V}_{fh} & , \text{ under aggressive mode} \\ \int f_2(V_{fh,DV}) - min[f_1(V_{fh,DV}), f_2(V_{fh,DV})]\, dV_{fh,DV} & , \text{ under conservative mode} \end{cases} \quad (13)$$

$$R_f = \begin{cases} f_1(V_{fh,DV}) dV_{fh,DV} \quad |V_{fh,DV} \geq \hat{V}_{fh} & , \text{ under aggressive mode} \\ min[f_1(V_{fh,DV}), f_2(V_{fh,DV})]\, dV_{fh,DV} & , \text{ under conservative mode} \end{cases} \quad (14)$$

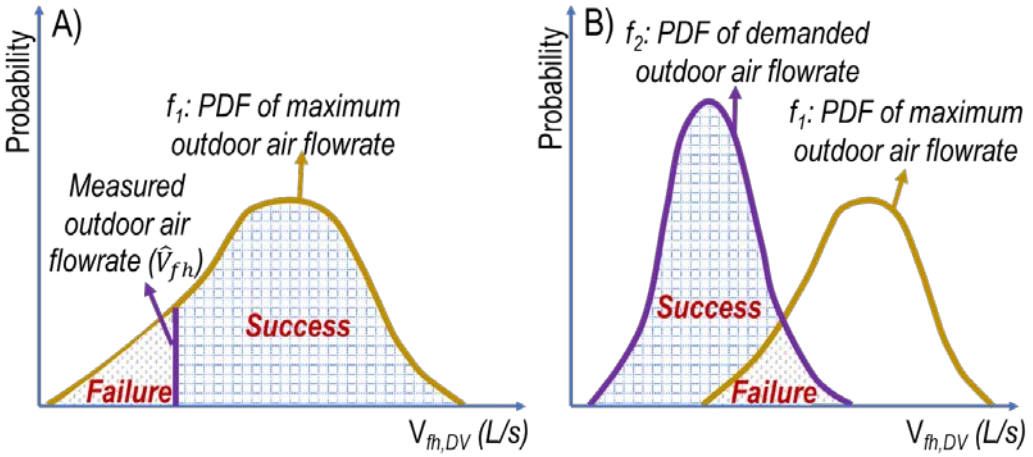

Fig. 10 Failure and success probability evaluation

(A. under aggressive mode B. under conservative mode)

Because E_b, E_w, R_f and R_s are all functions of the outdoor airflow rate ($V_{fh,DV}$), Eq. 1 can be rewritten as Eq. 15.

$$E_{nb} = \int \{R_s(V_{fh,DV})E_b(V_{fh,DV}) - R_f(V_{fh,DV})E_w(V_{fh,DV})\}\, dV_{fh,DV} \quad (15)$$

Fig. 11 illustrates the detailed steps of selecting the optimal control modes for individual AHUs. In the first step, the measurements, including supply air state, outdoor air state and heater status, are preprocessed using a low-pass filter (Eq. 16), to reduce the influence of random noises. Here, θ_{otp} is the filtered output. λ is the filtering weight factor. θ_{inp} is the actual measurement, and *j* and *j-1* are the current and previous sampling instants. In the second step, the failure risks and energy benefits of the different control modes are evaluated. If the cooling capacity of the MAU is estimated to be insufficient, the zone(s) with least heater energy use (estimated by Eq. 5) will adopt the conservative mode (i.e. the heaters of the corresponding AHU will be activated). In the third step, the decision is made, aiming to avoid unnecessary overcooling and reheating while ensuring that the system can operate at a low failure risk.

$$\theta_{otp,j} = \lambda\theta_{otp,j-1} + (1-\lambda)\theta_{inp,j} \tag{16}$$

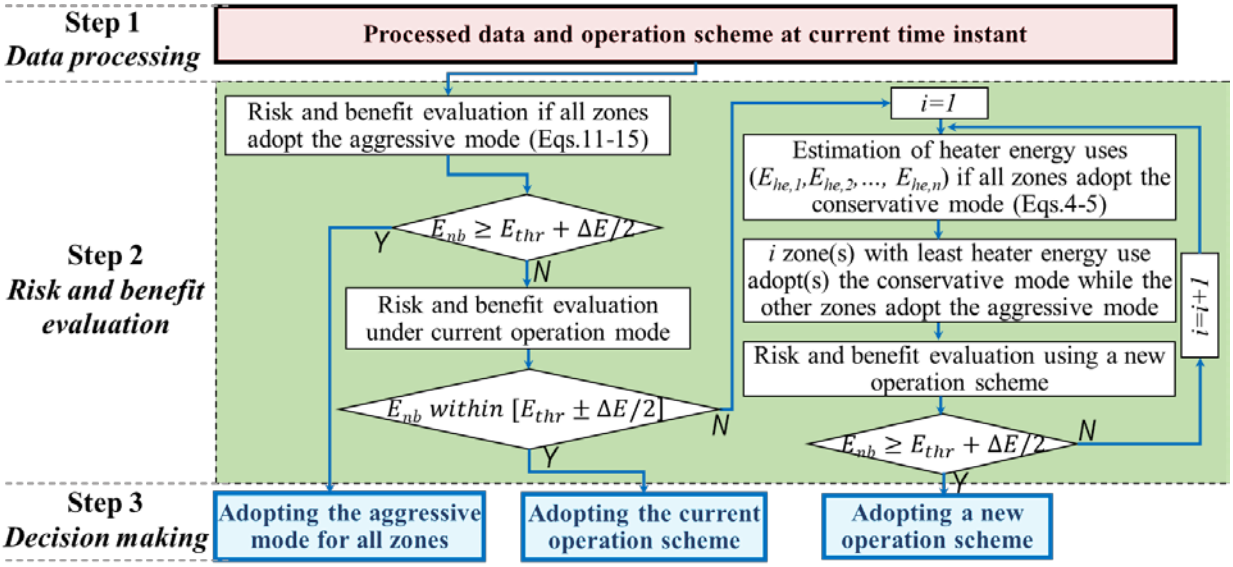

Fig. 11 Procedure of risk-based online decision making for individual AHUs

4 Test platform and identification of model coefficients

4.1 TRNSYS-MATLAB co-simulation testbed and test conditions

A virtual simulation platform was constructed using dynamic models developed in TRNSYS [34] to test the effectiveness of the proposed control strategy for cleanroom air-conditioning systems. To take advantage of its powerful computational capabilities, MATLAB was used to program the supervisory controller (which determines the optimal control mode on the basis of risks and benefits). The combined use of TRNSYS and MATLAB is presented in Fig. 12. The detailed physical models,

building envelop and major components (e.g. fans, hydraulic network, air ducts, cooling coils and heaters) of an air-conditioning subsystem are included in this dynamic simulation platform. The dynamic processes of hydraulics, heat transfer, airflow/pressure balancing, energy conservation and control were simulated for the entire system. The models used in the test platform were calibrated using real site operational data [35]. The building's thermal performance under the influences of weather, occupancy, and air-conditioning systems were characterized using the model type 56 in TRNSYS. The cleanroom air-conditioning subsystem mainly consists of an MAU and three AHUs, having same configuration shown in Fig. 1. This type of system is the most popular in real building projects of this kind and hence was selected for the testing and implementation of the proposed strategy. The simulated air-conditioning system was modified based on such a system from an actual pharmaceutical building in Hong Kong and the main design parameters (i.e. the inputs of the simulation platform) are presented in Table 2.

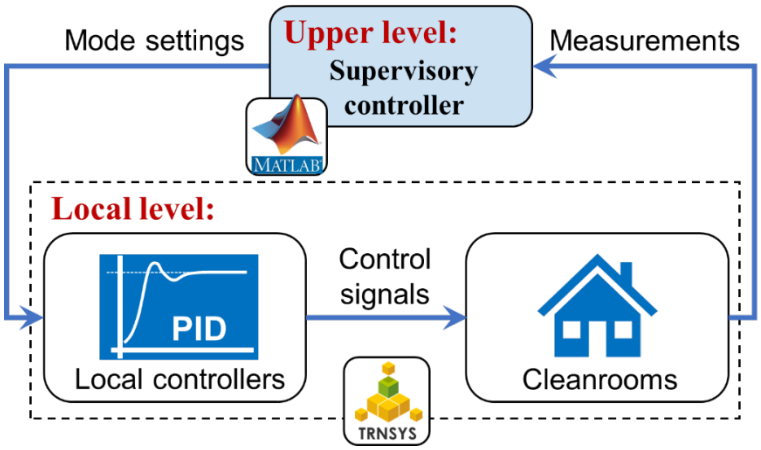

Fig. 12 TRNSYS-MATLAB co-simulation testbed for performance evaluation of control strategies.

The studied cleanrooms are designed as ISO class 8 [27]. The minimum total supply and outdoor airflow rates are designed as 20 ACH [28] and 2 ACH [36] respectively to meet the requirements of indoor cleanliness and pressurization. Three typical air-conditioned zones in this building were selected, served by one MAU and three AHUs. The upper limits of indoor temperature and relative humidity were set at 23 °C and 63% respectively, which are slightly lower than the upper limits of their allowable ranges. The actual MAU cooling capacity in operation was assumed to be degraded by 20% (i.e. 112 kW) compared with its rated cooling capacity. The reference control strategies and the proposed control strategy were all tested on the same platform to avoid the effects of model errors

and obtain reliable performance data of the proposed control strategy.

Table 2 Design room conditions, equipment configuration, and control requirements

Description	Parameter	Value
Envelope details	Wall ($W/m^2 \cdot K$)	1.5
	Roof ($W/m^2 \cdot K$)	0.8
	Window ($W/m^2 \cdot K$)	2.7
	Window to wall ratio (WWR)	0.2
Indoor design conditions	Temperature (°C)	21 ± 3
	Relative humidity (RH) (%)	55 ± 10
	Floor area (m^2)	Zone A: 105 (served by AHU-1) Zone B: 78.6 (served by AHU-2) Zone C: 99.8 (served by AHU-3)
	Height (m)	2.8
Indoor loads (sensible and latent heat)	Lighting (W/m^2)	13.9 + 0 (all zones)
	Occupants (W/m^2)	22 + 37 (all zones)
	Equipment (W/m^2)	151 + 55 (Zone A), 142 + 55 (Zone B), 144 + 52 (Zone C)
Outdoor and supply airflow rate	Outdoor air changes per hour (h^{-1})	≥2
	Supply air changes per hour (h^{-1})	≥20
Installed fans	Rated power (kW)	34 (MAU), 16 (AHU-1), 14 (AHU-2), 15 (AHU-3)
Cooling coils	Rated cooling capacity (kW)	140 (MAU), 38 (AHU-1), 32 (AHU-2), 35 (AHU-3)
Multi-stage heaters	Rated power of each heater (kW)	2.4 (AHU-1), 2.1 (AHU-2), 2.0 (AHU-3)
	Number of stages	5 (AHU-1), 4 (AHU-2), 5 (AHU-3)

To test the robustness of the proposed control strategy, measurement uncertainties (including biases and noises) were set for each type of sensor as summarized in Table 3.

Table 3 Sensor noises and biases introduced for case study

Measurement	Unit	Bias	Noise
MAU outlet temperature	°C	1.0	N (0,0.12)
MAU air flowrate	L/s	-54	N (0,5.43)
AHU-1 supply air temperature	°C	0.9	N (0,0.12)
AHU-1 supply air RH	%	2.0	N (0,0.78)
AHU-1 outdoor air flowrate	L/s	20	N (0,5.43)
AHU-1 supply air flowrate	L/s	-62	N (0,5.43)
AHU-2 supply air temperature	°C	-2.2	N (0,0.12)
AHU-2 supply air RH	%	1.5	N (0,0.76)
AHU-2 outdoor air flowrate	L/s	-17	N (0,5.43)
AHU-2 supply air flowrate	L/s	32	N (0,5.43)
AHU-3 supply air temperature	°C	-0.7	N (0,0.12)
AHU-3 supply air RH	%	-2.0	N (0,5.43)
AHU-3 outdoor air flowrate	L/s	-16	N (0,5.43)
AHU-3 supply air flowrate	L/s	-45	N (0,5.43)

4.2 Identification of model coefficients for risk and benefit evaluation

The normal operational data for calculating the model coefficients (Eqs. 3-4, 10) were generated by simulating the cleanroom air-conditioning systems over a wide range of ambient and indoor load conditions. Two sets of operational data were generated: one was free of measurement errors, while the other was obtained after introducing the measurement errors. Fig. 13 shows the theoretical and adaptive models of the maximum outdoor airflow and demanded outdoor air flowrate. It can be seen that due to the MAU performance degradation and measurement uncertainties, the predicted values deviate far from the theoretical values under the given working conditions. The coefficients of the theoretical and adaptive maximum and demanded outdoor air flowrate models (Eqs. 4-5) are listed in Table 4. The coefficients of the adaptive models are uncertain while those of the theoretical models are deterministic.

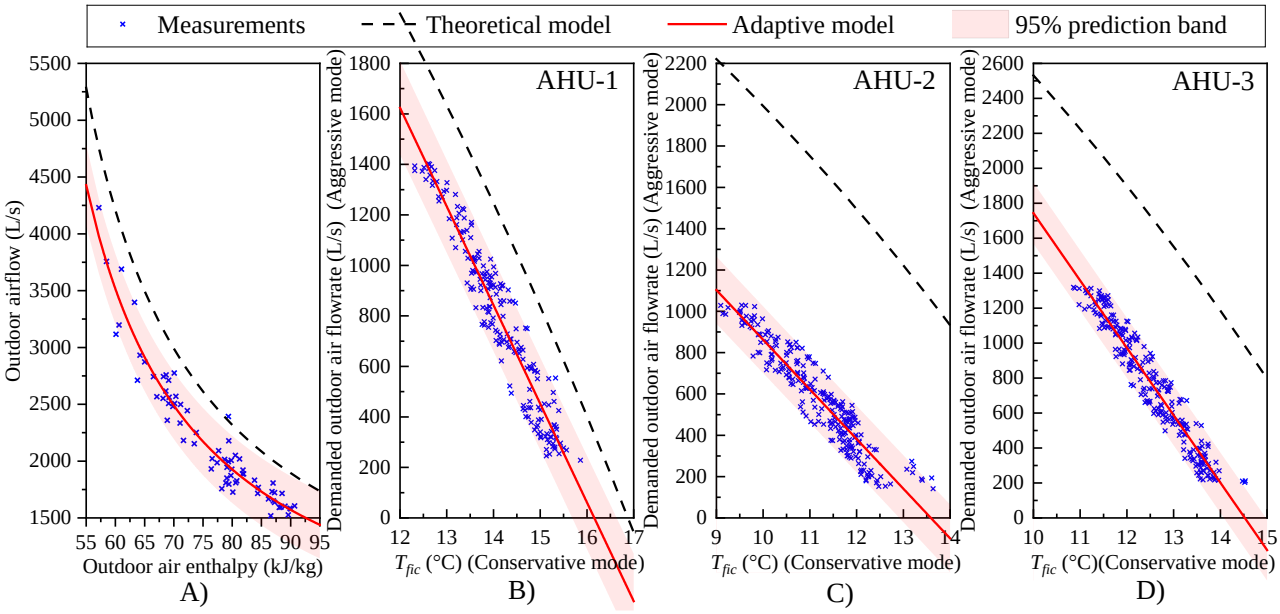

Fig. 13 Comparison of theoretical and adaptive models

(A. maximum outdoor air flowrate models; B-D. demanded outdoor air flowrate models for AHU-1, AHU-2 and AHU-3)

Table 4 The coefficients of theoretical and adaptive models

Coefficient	Identified value for theoretical models (*deterministic value*)	Identified value for adaptive models (*with 95% confidence bounds*)
a_1	4.35×10^5	3.40×10^5 (3.15×10^5, 3.65×10^5)
a_2	-3057	-2294 (-2626, -1963)
$b_{1,1}$	-387.8	-390.7 (-406.8, -374.6)
$b_{2,1}$	6630	6312 (6084, 6541)
$b_{1,2}$	-257.2	-240.3 (-251.5, -229.1)
$b_{2,2}$	4566	3266 (3140, 3391)
$b_{1,3}$	-368.6	-385.4 (-398.4, -372.5)
$b_{2,3}$	6302	5598 (5435, 5760)

The fan power model was fitted using the “measured” outdoor airflow as shown in Fig. 14. Eq. 17 was used to estimate the fan power under a given outdoor airflow.

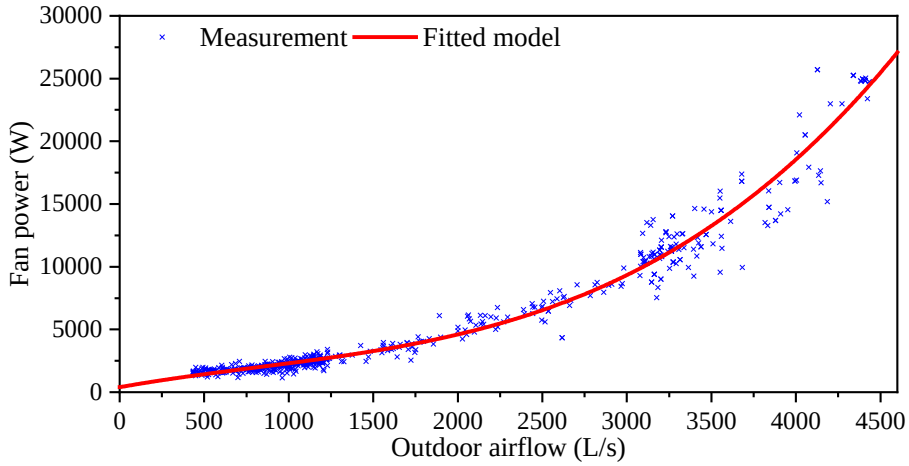

Fig. 14 Estimated fan power using the measured outdoor airflow

$$P_{fan} = 3.4 \times 10^{-7}\, V_{fh}^3 - 0.0008 V_{fh}^2 + 2.39 V_{fh} + 398.47 \quad (17)$$

5 Performance tests and evaluation of proposed risk-based optimal control strategy

5.1 Reference control strategies and load conditions

To evaluate the control performance and energy efficiency of the cleanroom air-conditioning system using the proposed risk-based online optimal control strategy (Strategy #5), four control strategies were selected for comparison as shown in Table 5. Strategies #1, #2 and #3 each adopt a single control mode while Strategies #4 and #5 enable dynamic selection of the control mode from multiple options during operation. Strategy #1 adopts IC, the most commonly used control strategy in cleanroom air-conditioning systems. The MAU outlet temperature is controlled at 18 °C by modulating the MAU cooling coil valve. Zone temperature and relative humidity are controlled by adjusting the AHU cooling coil valve and heater output. Strategy #2 adopts PD, and has the same mechanism and settings as the PD mode of Strategy #5. In Strategy #3, the control mode is DV, under the same mechanism and settings as the DV mode of Strategy #5. Meanwhile, Strategy #4 allows both DV and PD modes, and selects between them by comparing their predicted energy performance based on the theoretical models. The difference between Strategy #4 and #5 is that the component performance degradation and measurement uncertainties are not considered in Strategy #4.

Note that only local process controls are involved for Strategies #1, #2 and #3 while both local-level process controls and upper-level supervisory controls are required for Strategies #4 and #5. For Strategies #3, #4 and #5, when the MAU cooling demand exceeds its capacity, control failure may

occur (i.e. the indoor temperature and relative humidity will go outside of the allowable ranges). In this study, to ensure the control reliability of the systems, subcooling and reheating processes of the AHU are adopted for Strategy #3 when control failure occurs (for a minimum of 10 mins). For Strategies #4 and #5, inside the critical zone (i.e. the zone with least estimated heater energy use), the control mode is switched from aggressive to conservative when control failure occurs. The threshold (E_{thr}) and dead band (ΔE) in Eq. 1 are selected as 0 kW and 5 kW respectively.

Table 5 Description of the control strategies

	Strategy	Description	Supervisory control
Reference strategies	Strategy #1	MAU outlet temperature is controlled at 18 °C. Outdoor air flowrate is set at minimum. The system resorts to subcooling and reheating processes for indoor air temperature and humidity control.	×
	Strategy #2	MAU outlet temperature is controlled at 13 °C. Outdoor air flowrate is set at minimum. The system resorts to subcooling and reheating processes when the indoor latent load is high.	×
	Strategy #3	MAU outlet temperature is controlled at 13 °C. Outdoor air flowrate is adjusted according to the indoor latent load.	×
	Strategy #4	MAU outlet temperature is controlled at 13 °C. The system selects the control mode by comparing energy performances of modes based on the theoretical models. Performance degradation and measurement uncertainties are not considered using this strategy.	√
Proposed	Strategy #5	MAU outlet temperature is controlled at 13 °C. The system selects the control mode based on the risk-based online optimal decision-making scheme. Performance degradation and measurement uncertainties are considered using this strategy.	√

A typical day in Hong Kong was selected to test the performance of the proposed control strategy. The ambient conditions and load settings are shown in Fig. 15. The patterns of lighting and occupants of all three zones were set as constants (i.e. 1.0 and 0.5 respectively) on the test day.

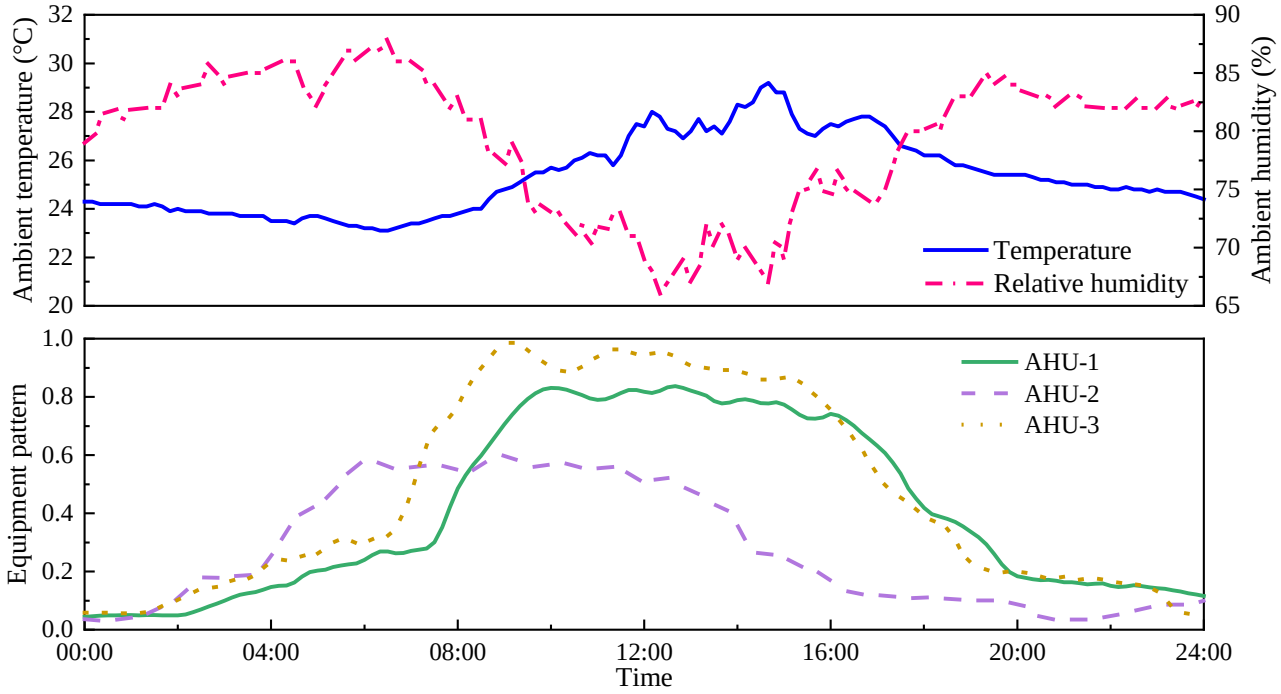

Fig. 15 Ambient conditions and load patterns for performance evaluation

Note: The load patterns are given as fractions of their respective design values

5.2 Energy performance comparison of proposed and reference strategies

To demonstrate the mechanism of energy-efficient control under the proposed control strategy, the outdoor air flowrate, cooling and heating output in the dynamic simulation are compared with the reference strategies. Fig. 16 shows the outdoor air flowrates and cooling value of the MAU using the different strategies. Strategies #1 and #2 always induced the minimum required outdoor air flowrate, and the MAU cooling valve opening was less than in the other three control strategies throughout the day. Under Strategies #3, #4 and #5, the minimum required outdoor air flowrates were induced for a short period (00:00-02:00) during which the indoor latent load in the three zones was low, but these outdoor air flowrates were above their lower limits for most of the day (02:00-24:00) due to the need of dehumidification in the MAU. However, for Strategy #3, during 09:40-16:30 the cooling valve of the MAU was frequently fully open, indicating that the dehumidification capacity of the MAU was insufficient to handle the complete indoor latent load of all three zones. The insufficient MAU capacity resulted in a large amount of outdoor air being introduced, leading to system control failure. For Strategy #4, the cooling valve of the MAU was likewise fully open during 09:40-10:00, resulting in a brief episode of control failure. This failure can be attributed to the neglect of measurement uncertainties and component performance degradation in Strategy #4, which jeopardized the

accuracy of the estimated MAU cooling demand and cooling capacity. For Strategy #5, the cooling valve of the MAU was never fully open, indicating that its cooling capacity met its cooling demand throughout the day thanks to the judicious choice of control modes for individual zones.

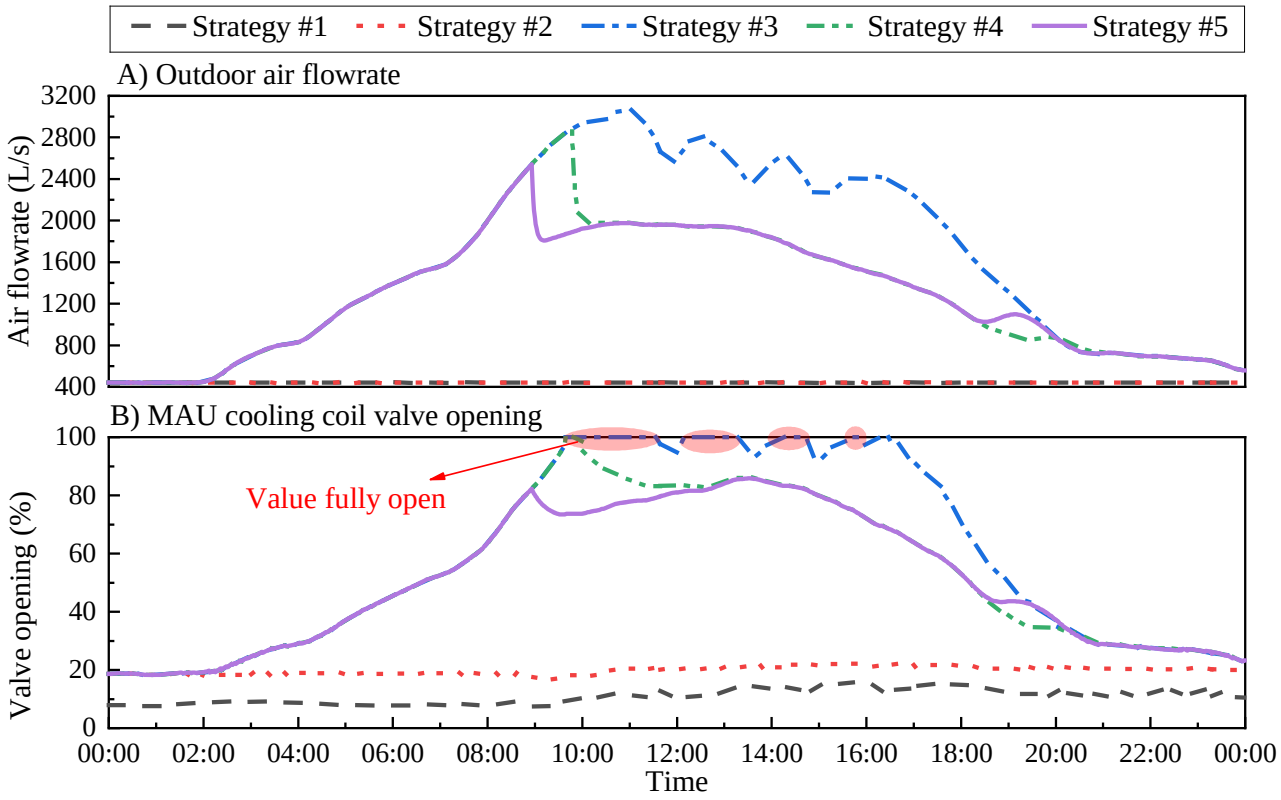

Fig. 16 Outdoor air flowrate and cooling valve opening of MAU using five control strategies

For the sake of energy efficiency of air-conditioning systems, unnecessary sub-cooling and reheating processes should be avoided. Fig. 17 shows the heater stages of the AHUs using the five control strategies. For Strategy #1, the three AHUs experienced overcooling and reheating counteraction processes throughout the day. For Strategy #2, overcooling and reheating were avoided during certain times (e.g. from 00:00 to 02:00) compared with Strategy #1 under conditions of low indoor latent load. For Strategy #3, the three AHUs likewise underwent counteraction processes due to the insufficient MAU cooling capacity around 10:00-16:30. For Strategies #4 and #5, the counteraction processes only occurred in Zone C (served by AHU-3), while the heaters in the other two AHUs (associated with Zone A and Zone B) were not activated at any time during the day. However, the activation of heaters was delayed under Strategy #4 compared with Strategy #5. The schemes for control mode selection (represented by the heater output) differed between Strategies #4 and #5 due to the existence of measurement uncertainties and different decision-making schemes.

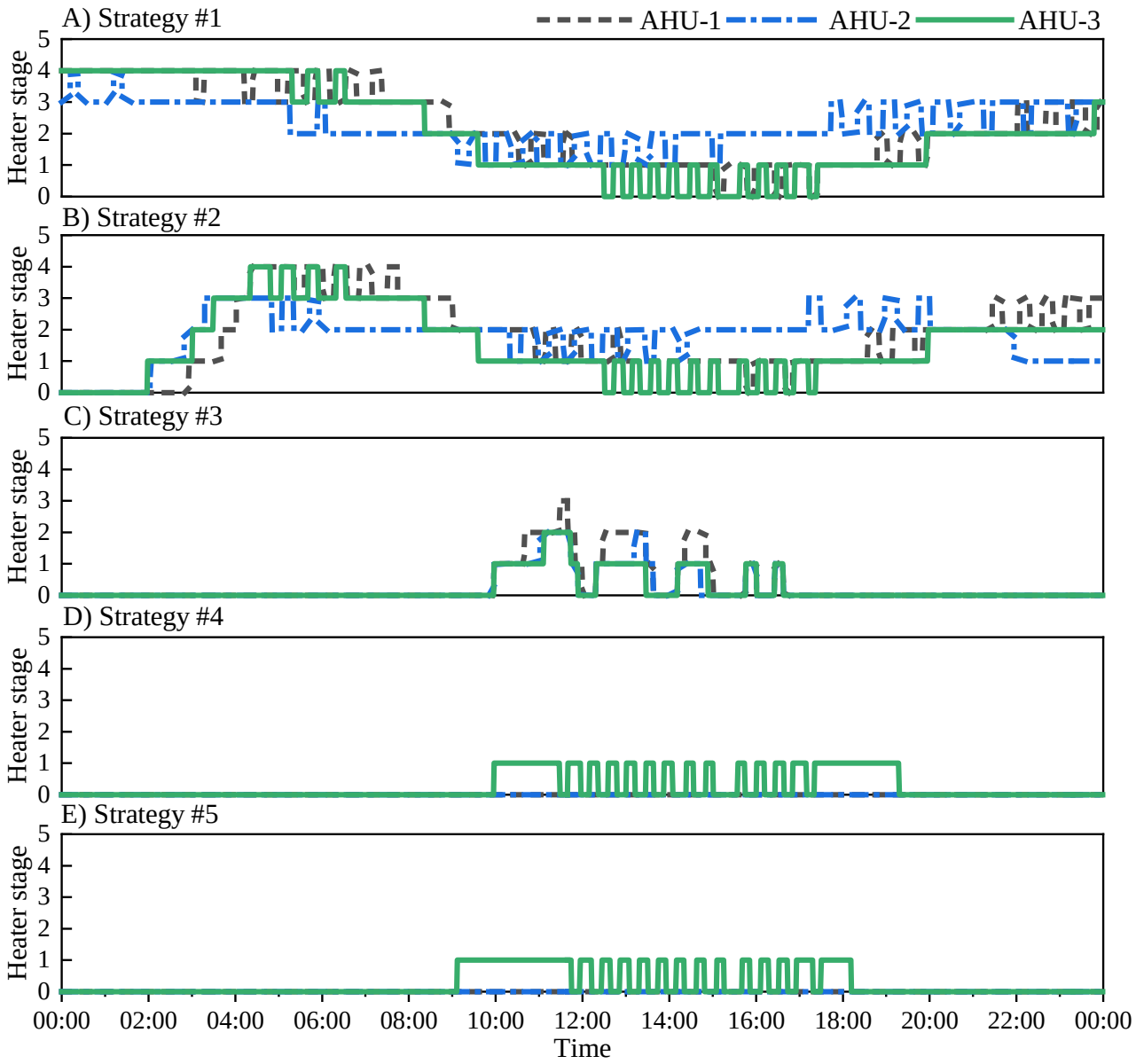

Fig. 17 Heater stage of AHUs using five control strategies

The energy consumption terms, including the cooling coils, heaters and fans as well as the entire air-conditioning systems, using the five control strategies are shown in Table 6. Compared with the conventional Strategy #1, Strategy #2 saved both the cooling and heating energy by 5.8% and 24.0% due to the avoidance of overcooling and reheating under low space latent load. For Strategies #3, #4 and # 5, the heating energy use was significantly decreased by 89.5%, 96.5% and 96.6% respectively due to the decoupling temperature and humidity control loops. However, the cooling energy use increased by 18.4%, 5.9% and 5.4% respectively due to the introduction of excessive high-enthalpy outdoor air flowrates. Compared with Strategy #1, the overall energy savings of Strategies #2, #3, #4 and #5 were 9.3%, 9.2%, 19.4% and 19.9%, respectively.

Table 6 Energy consumptions using five control strategies on the test day

	Strategy #1	Strategy #2	Strategy #3	Strategy #4	Strategy #5
MAU fan consumption (kWh)	31.7	31.7	99.7	73.9	71.0
MAU cooling consumption (kWh)	110.5	180.1	661.5	532.8	523.5
AHU cooling consumption (kWh)	552.1	444.1	122.7	168.9	174.8
AHU heating consumption (kWh)	345.6	262.6	36.4	12.0	11.8
AHU fan consumption (kWh)	259.2	259.2	259.2	259.2	259.2
Overall energy consumption (kWh)	1299.1	1177.8	1179.6	1046.8	1040.2
Cooling energy saving (%)	-	5.8	-18.4	-5.9	-5.4
Heating energy saving (%)	-	24.0	89.5	96.5	96.6
Overall energy saving (%)	-	9.3	9.2	19.4	**19.9**

5.3 Control reliability of proposed strategy compared with reference strategies

For cleanroom air-conditioning systems, the reliability of indoor temperature and relative humidity control is a major issue. Reliability implies that the indoor temperature and relative humidity can be controlled within the allowable ranges during operation, meaning that satisfactory services can be offered. Fig. 18 shows the indoor air temperature and relative humidity profiles of the three zones using the five control strategies. Generally, the indoor air temperature and relative humidity were controlled within the allowable range using Strategies #1, #2 and #5. However, for Strategies #3 and #4, control failure occurred around 09:50-10:10 due to the insufficient MAU cooling capacity for dehumidification. For Strategy #5, the indoor air temperature and relative humidity of the zones were controlled within the allowable ranges throughout the test day. This indicates that the proposed risk-based online optimal control strategy can fulfill the requirements of indoor environment control and thus offer satisfactory service.

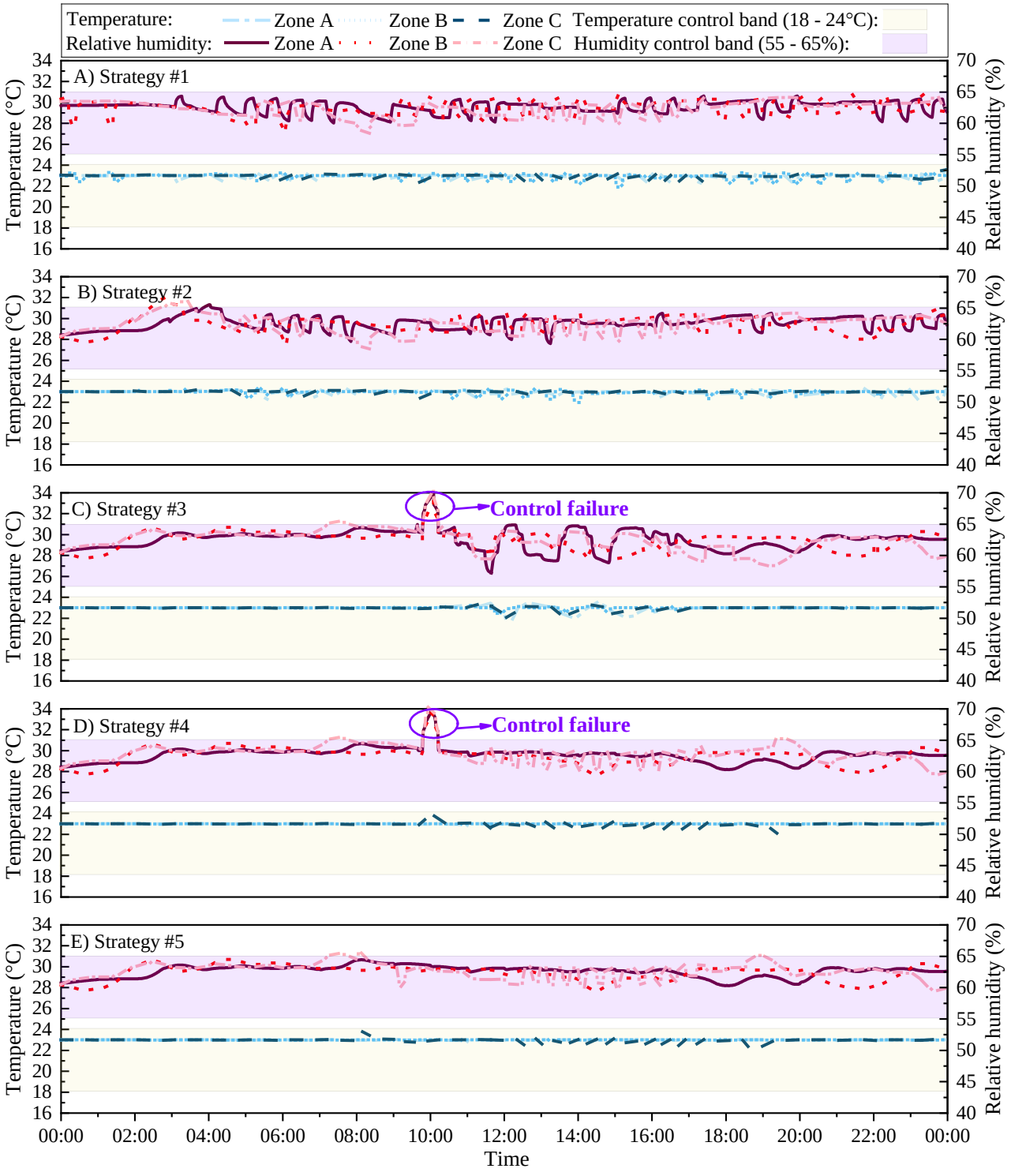

Fig. 18 Indoor air temperature and relative humidity profiles using five control strategies

Fig. 19 shows the control mode selection (i.e. the number of zones adopting the aggressive mode) of Strategies #4 and #5, demonstrating the importance of considering the component performance degradation and measurement uncertainties in upper-level supervisory control. It can be seen that the systems adopting Strategy #5 shifted from the aggressive to the conservative control mode in the critical zone in advance (i.e. at 08:55) to avoid control failure, based on the risk assessment. In

contrast, aggressive mode failure occurred under Strategy #4, due to the inaccurate estimation of MAU cooling demand and capacity. In addition, compared with Strategy #5, the mode shifting was delayed under Strategy #4, causing more energy waste.

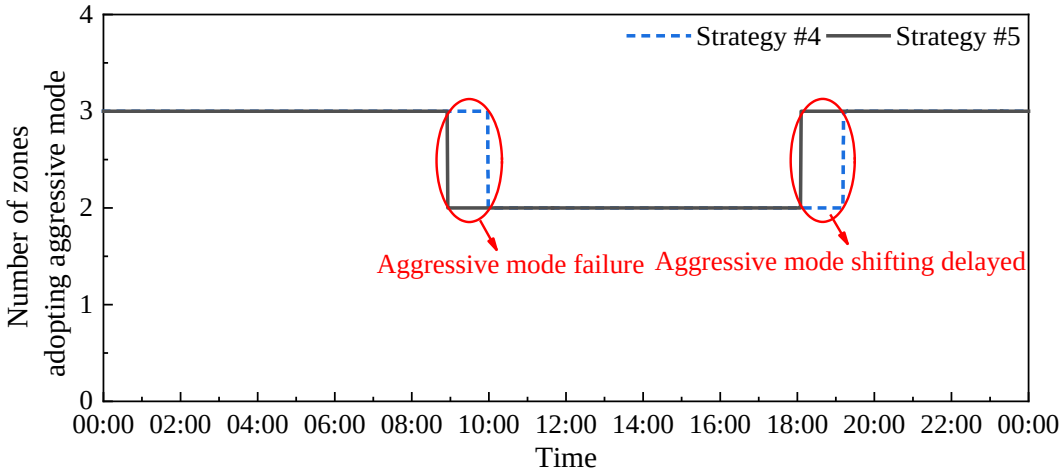

Fig. 19 Number of zones adopting aggressive mode using Strategies #4 and #5

Fig. 20 presents the risks and expected net energy benefits in the decision-making process when adopting Strategy #5, evaluated under the assumption that all zones adopt the aggressive mode. The selected control modes for individual zones in the decision-making process are shown in Table 7. When the space latent load stayed at a low level (i.e. in periods 1 and 3), the failure probability was also estimated to be low, if all zones in the aggressive mode. Therefore, all of the zones selected this mode because of the high expected net energy benefits estimated by the decision-making scheme. When the indoor latent load increased (i.e. in period 2), the control strategy determined the control mode for each zone based on the expected net energy benefits. Zone C (served by AHU-3), which was estimated to use the least heater energy (Eqs. 4-5), switched from the aggressive to the conservative mode, to ensure that the other two zones could operate under the aggressive mode successfully.

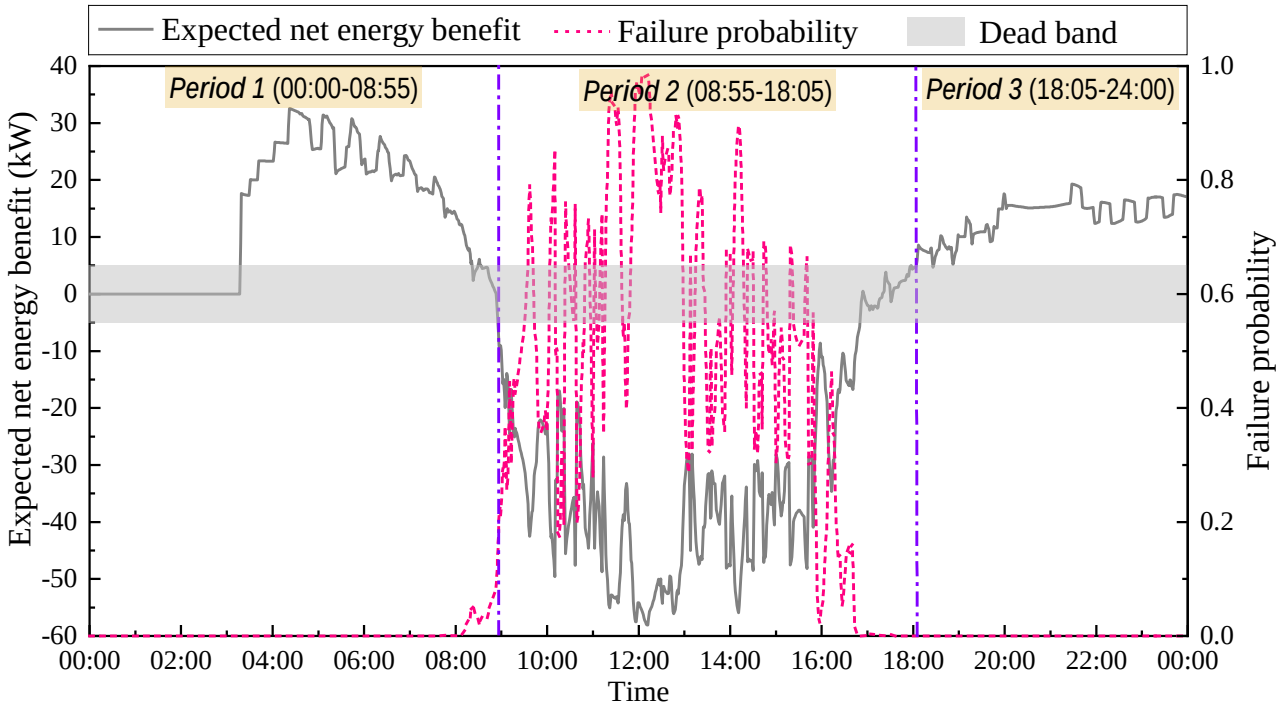

Fig. 20 Risks and expected net energy benefits in the decision-making process

Table 7 Control mode in different periods selected by risk-based decision-making approach

	Period 1 (00:00-08:55)	Period 2 (08:55-18:05)	Period 3 (18:05-24:00)
Zone A	Aggressive mode	Aggressive mode	Aggressive mode
Zone B	Aggressive mode	Aggressive mode	Aggressive mode
Zone C	Aggressive mode	***Conservative mode***	Aggressive mode

6 Discussion

Energy-efficient control strategies in the operation of cleanroom air-conditioning systems reduce energy consumption and operational costs, and maintain more reliable control of the cleanroom environment. The results of performance tests indicated that the proposed risk-based control strategy appropriately selected or shifted the control modes to achieve energy-efficient and reliable operation of environmental control systems. This is especially important for industrial applications, where the integrity of cleanroom production environments must be preserved and highly sophisticated and knowledge-intensive manufacturing processes are involved.

Based on the performance tests of the developed strategy and a review of the existing literature, several issues still need to be addressed in further studies for the successful implementation of the risk-based control strategy in practice:

1. Concerning measurement, there is a need to collect data regularly under different operation states

(i.e. failure or success) of the control modes. The data can be used to update the component performance model and improve the accuracy of risk/benefit evaluation. For instance, in the selected test case, if aggressive control fails, the outdoor air flowrate induced in practice can be obtained from actual measurements. The flowrate measurements can then be used for quantifying the energy waste of the aggressive mode.

2. Concerning the model prediction, there is a need for sensitivity and uncertainty analysis to identify the impacts of errors of different sensor on the performance of the control strategies. This would reduce the need for data collection, and simplify the risk/benefit analysis, hence facilitating online decision-making. For instance, Shan et al. [37] conducted a sensitivity analysis of measurements and found that the accuracy of the outdoor airflow meter had the most significant impact on the performance of the ventilation control strategy.

3. The successful implementation of the risk-based control strategy requires the predictive models to be adaptive to the changes of working conditions. In this study, the parameters of the models were identified using operational data under normal conditions. There is a need for a robust approach to self-tune the coefficients/parameters of predictive models in cases of control failure. In practical applications, control failure (i.e. due to improper decision making) may occur due to either changes of working conditions or sensor errors. An online learning and estimation approach is required to re-calculate and update the coefficients of the predictive models and preserve the model accuracy when the working conditions change or the component performance is degraded.

4. The cost function (for evaluating risk and benefit) for decision-making must be modified for cleanrooms requiring higher cleanliness levels. In such applications, due to the higher requirements of environmental control, the tolerance for control failure is lower. The cost function must be updated to ensure that the systems operate with high reliability. This can be achieved by properly setting the penalty for unsatisfactory service [11].

7 Conclusions

A risk-based online optimal control strategy for multi-zone cleanroom air-conditioning systems was proposed. As the core of the control strategy, an online optimal decision-making scheme was developed based on a compromise between the risks and benefits of various control modes, to select

the optimal mode, allowing for component performance degradation and measurement uncertainties. The proposed control strategy was tested and implemented on a simulation platform. Based on the results of the tests and implementation, some detailed conclusions can be drawn:

- The proposed strategy can successfully determine the optimal control mode allowing for component performance degradation and measurement uncertainties, enabling air-conditioning systems to operate with both high reliability and energy efficiency.
- The online optimal decision-making scheme is effective in quantifying the correlations between different control modes and evaluating the energy benefits and failure risks of these modes under uncertainties.
- In the test period, the proposed strategy based on risk-assessment achieved approximately 20% overall energy saving compared with interactive control, the most commonly used method.

The proposed risk-based online decision-making approach can also be applied for other systems with multiple control modes that may require mode shifting under certain conditions. In real applications, due to various uncertainties, engineers usually prefer to select a conservative/safe mode rather than an aggressive mode (i.e. with more energy-saving potential but higher risks), to ensure highly reliable operation [38]. In this study, a quantification method of risks and benefits was developed for decision-making accounting for measurement uncertainties, offering a promising means for engineers to exploit the potential benefits of control mode shifting.

Notably, the coefficients of the adaptive models were fitted using building simulation tools and implemented in specific cases in this study. In real applications, operational data of typical working conditions under different control modes are needed to identify these coefficients.

It is also worth noting that in this study, in the case of mode failure, a penalty was incurred by assuming that 100% outdoor airflow is induced associated with simultaneous cooling and heating processes, forcing the system to provide satisfactory environmental control. In real applications, the penalty should be properly set according to the environmental control requirements.

More importantly, on-site implementation and comprehensive validation of the proposed online control strategy and the corresponding control schemes, are needed under real conditions matching the system requirements. On-site test results will be essential for updating the strategy to achieve

satisfactory performances in practical applications. Further tests and validation of the proposed online control strategy in real buildings would be of considerable value in future studies.

Acknowledgement

The research presented in this paper is financially supported by a grant (152075/19E) of the Research Grant Council (RGC) of the Hong Kong SAR.

Appendix A. Correlations between $T_{fic,PD}$ and $V_{fh,DV}$

The correlations between $T_{fic,PD}$ and $V_{fh,DV}$ are based on the assumption that the MAU outlet air state is in a steady state (e.g. 13 °C, 95%). When the system operates using the aggressive control mode, the demanded outdoor airflow is proportional to the space latent load as shown in Eq. A.1. When the system resorts to overcooling and reheating to remove indoor latent heat using the conservative mode, $T_{fic,PD}$ is the apparatus dewpoint. The moisture content ($w_{out,PD}$) is linearly related to apparatus dewpoints [10]. Therefore, the AHU cooling coil outlet temperature has negative linear relationship to the indoor latent cooling load (Q_{lat}) and demanded outdoor airflow of the aggressive mode (as shown in Eq. A.2). Eq. 4 can then be derived by combining Eqs. A.1-A.2.

$$V_{fh,DV} \propto Q_{lat} \tag{A.1}$$

$$T_{fic,PD} \propto w_{out,PD} \propto -Q_{lat} \propto -V_{fh,DV} \tag{A.2}$$

Reference

[1] Mathew P. An estimate of energy use in laboratories, cleanrooms, and data centers in New York. Lawrence Berkeley Natl Lab Report, Berkeley, US 2008.

[2] Kircher K, Shi X, Patil S, Zhang KM. Cleanroom energy efficiency strategies: Modeling and simulation. Energy Build 2010;42:282–9.

[3] Mills E. Energy efficiency in California laboratory-type facilities. Lawrence Berkeley Natl Lab Report, Berkeley, US 1996.

[4] Wu XP, Johnson P, Akbarzadeh A. Application of heat pipe heat exchangers to humidity control in air-conditioning systems. Appl Therm Eng 1997;17:561–8.

[5] Tsao JM, Hu SC, Xu TF, Chan DYL. Capturing energy-saving opportunities in make-up air

systems for cleanrooms of high-technology fabrication plant in subtropical climate. Energy Build 2010;42:2005–13.

[6] Shan K, Wang SW. Energy efficient design and control of cleanroom environment control systems in subtropical regions–A comparative analysis and on-site validation. Appl Energy 2017;204:582–95.

[7] Jouhara H. Economic assessment of the benefits of wraparound heat pipes in ventilation processes for hot and humid climates. Int J Low-Carbon Technol 2009;4:52–60.

[8] Brown WK. Makeup air systems energy-saving opportunities. ASHRAE Trans 1990;96.

[9] Zhuang CQ, Wang SW, Shan K. Adaptive full-range decoupled ventilation strategy and air-conditioning systems for cleanrooms and buildings requiring strict humidity control and their performance evaluation. Energy 2019;168:883–96.

[10] ASHRAE. ASHRAE Handbook: Fundamentals. Am Soc Heating, Refrig Air Cond Eng Atlanta, GA 2013.

[11] Zhuang CQ, Wang SW, Shan K. Probabilistic optimal design of cleanroom air-conditioning systems facilitating optimal ventilation control under uncertainties. Appl Energy 2019;253:113576.

[12] Wang SW, Ma ZJ. Supervisory and optimal control of building HVAC systems: A review. HVAC&R Res 2008;14:3–32.

[13] Nassif N, Kajl S, Sabourin R. Optimization of HVAC control system strategy using two-objective genetic algorithm. HVAC&R Res 2005;11:459–86.

[14] West SR, Ward JK, Wall J. Trial results from a model predictive control and optimisation system for commercial building HVAC. Energy Build 2014;72:271–9.

[15] Ferreira PM, Ruano AE, Silva S, Conceicao EZE. Neural networks based predictive control for thermal comfort and energy savings in public buildings. Energy Build 2012;55:238–51.

[16] Min YR, Chen Y, Yang HX. A statistical modeling approach on the performance prediction of indirect evaporative cooling energy recovery systems. Appl Energy 2019;255:113832.

[17] Yan B, Li X, Malkawi AM, Augenbroe G. Quantifying uncertainty in outdoor air flow control and its impacts on building performance simulation and fault detection. Energy Build 2017;134:115–28.

[18] Goyal S, Ingley HA, Barooah P. Effect of various uncertainties on the performance of occupancy-based optimal control of HVAC zones. 2012 IEEE 51st IEEE Conf Decis Control 2012:7565–70.

[19] Yu Y, Woradechjumroen D, Yu D. A review of fault detection and diagnosis methodologies on air-handling units. Energy Build 2014;82:550–62.

[20] Yang X Bin, Jin XQ, Du ZM, Fan B, Zhu YH. Optimum operating performance based online fault-tolerant control strategy for sensor faults in air conditioning systems. Autom Constr 2014;37:145–54.

[21] Wang SW, Chen YM. Fault-tolerant control for outdoor ventilation air flow rate in buildings based on neural network. Build Environ 2002;37:691–704.

[22] Jin X, Du Z. Fault tolerant control of outdoor air and AHU supply air temperature in VAV air conditioning systems using PCA method. Appl Therm Eng 2006;26:1226–37.

[23] Kuklicke C, Demeritt D. Adaptive and risk-based approaches to climate change and the management of uncertainty and institutional risk: The case of future flooding in England. Glob Environ Chang 2016;37:56–68.

[24] Hult GTM, Craighead CW, Ketchen David J J. Risk uncertainty and supply chain decisions: a real options perspective. Decis Sci 2010;41:435–58.

[25] Peterman RM, Anderson JL. Decision analysis: a method for taking uncertainties into account in risk-based decision making. Hum Ecol Risk Assess An Int J 1999;5:231–44.

[26] Ellingwood BR, Wen Y. Risk-benefit-based design decisions for low-probability/high consequence earthquake events in Mid-America. Prog Struct Eng Mater 2005;7:56–70.

[27] ISO. 14644-1: 2015, Cleanrooms and associated controlled environments–Part 1: Classification of air cleanliness by particle concentration. Int Organ Stand Geneva, Switz

2015.

[28] PG&E. Energy efficiency baselines for cleanrooms. San Fr Pacific Gas Electr Co 2010.

[29] Turk BH, Grimsrud DT, Brown JT. Commercial building ventilation rates and particle concentrations 1988.

[30] Law AKY, Chau CK, Chan GYS. Characteristics of bioaerosol profile in office buildings in Hong Kong. Build Environ 2001;36:527–41.

[31] Huang GS, Wang SW, Xiao F, Sun Y. A data fusion scheme for building automation systems of building central chilling plants. Autom Constr 2009;18:302–9.

[32] Smirnov N V, Dunin-Barkowski I V. Mathematische statistik in der technik. Dtsch Verl Der Wissenschaften 1963.

[33] Salimifard P, Delgoshaei P, Xu K, Freihaut JD. Comparison of actual supply air fan performance data to ASHRAE 90.1 Standard-2010 and DOE Commercial Reference Buildings part load fan energy use formula. ASHRAE/IBPSAUSA Build Simul Conf 2014.

[34] TRNSYS. Transient System Simulation Tool. Univ Wisconsin, USA Sol Energy Lab 2017.

[35] Wang SW. Dynamic simulation of building VAV air-conditioning system and evaluation of EMCS on-line control strategies. Build Environ 1999;34:681–705.

[36] ASHRAE 62.1. Ventilation for Acceptable Indoor Air Quality. Am Soc Heating, Refrig Air-Conditioning Eng Atlanta, GA 2016.

[37] Shan K, Wang SW, Xiao F, Sun YJ. Sensitivity and uncertainty analysis of measurements in outdoor airflow control strategies. HVAC&R Res 2013;19:423–34.

[38] Teng SG, Ho SM. Failure mode and effects analysis. Int J Qual Reliab Manag 1996.